2014

Finite Element Simulation of Fillet Welds: Influence of Weld Contact Angle and Metallurgical Phase Changes on Residual Stresses

Chao Zhang
Lehigh University

Finite Element Simulation of Fillet Welds: Influence of Weld Contact Angle and Metallurgical Phase Changes on Residual Stresses

by

Chao Zhang

A Thesis

Presented to the Graduate and Research Committee

of Lehigh University

in Candidacy for the Degree of

Master of Science

in

Mechanical Engineering

Lehigh University

August 2014

This thesis is accepted and approved in partial fulfillment of the requirements for the Master of Science.

_____

Date

_____

Thesis Advisor

_____

Chairperson of Department

Acknowledgments

The author wishes to express his appreciation and thanks to his advisor, Prof. Herman F. Nied, for his continuous support and valuable guidance throughout this M.S. study.

The author also wishes to thank his family for their continuous encouragement and support. Thanks are also due to my friends for their kind contributions and support.

Table of Contents

List of Figures

Abstract

Thermomechanical simulation of welding is very useful for developing a better understanding of how residual stresses evolve during welding operations. Detailed information about welding residual stresses can be of great benefit for better predictions of fatigue behavior in welded structures, since it is generally recognized that improvements in weld quality and reduction in welding residual stresses are necessary for increased fatigue life.

In this study, we use computational simulation to simulate the residual stress distribution after welding. Of particular interest are the local stresses at the edge of a fillet weld; a location known to be the most likely site for fatigue crack initiation. Three models with different fillet geometry are developed to investigate how the geometry of fillet weld influences the residual stress under different clamping conditions and with different material properties. The fillet geometry not only affects the residual stresses directly, because of the stress concentration due to the geometry change, but also affects the residual stresses indirectly, through metallurgical changes in the Heat Affect Zone (HAZ). The results near the weld toe, where stress concentration effects are strongest, are are of the greatest interest. The convergence and accuracy of the stress results are verified by systematically preforming repeated simulations using different mesh refinements close to the weld toe.

Chapter 1

Introduction

Fusion welding is a relatively simple joining process: where essentially large numbers of atoms of the constituent materials being joined come together in an equilibrium spacing [1]. However, as will be shown in this study, the thermomechanical details associated with welding are quite complex. The focus in this study is the evolution of residual stresses at the edges of a fillet weld. The state of stress at this location, i.e., the toe of the fillet weld, is of great significance in welded structures, since this is location where fatigue cracking is most often observed. The residual stresses associated with welding are strongly influenced by the local geometry of the fillet (stress concentration effect), mechanical boundary conditions, heat transfer, and metallurgical phase changes.

Studies of fatigue behavior in welded structures have confirmed the import role that welding process parameters play in controlling fatigue reliability. There have been many research projects that have closely looked at the interaction between welding residual stresses and fatigue life in recent decades, e.g., [2-5]. [5] indicated that fatigue crack growth rate is dominated by high residual stress and also is related with crack orientation and distance from weld tow. High residual stress often occurred near the toe of fillet and was often responsible for early fatigue crack initiation. Many experiences show crack often happen in the Heat Affected Zone (HAZ), close to the welding toe [6]., because a high residual stress would generate as a result of the temperature gradient of

HAZ during cooling down. Clamped-clamp, clamped-free, and free-free boundary conditions also influence stresses distribution and fatigue crack initiation [4].

Finite element computational techniques provide a convenient means for simulating and analyzing welding processes [7-11]. In many respects, welding simulation software provides a specialized CAE (Computer Aided Engineering) tool, based on highly nonlinear thermomechanical properties. The welding material properties obtained from welding experiments provide the data used in the finite element computer simulation models needed to predict welding residual stresses [7]. In most welding finite element simulations, empirical models are used to avoid directly simulating the complex fluid/structure interactions that occurs in the molten zone during the transition from solid to liquid and re-solidification during cool down.

Of particular interest in this study, is explaining the large difference in the residual stress results between austenitic stainless steel and carbon steel after welding. Experiments tend to show that welds in austenitic stainless steel have much higher residual stresses near the fillet weld toe after cool down, when compared with carbon steel. The differences in residual stresses, for identical weld geometries, can be attributed to the metallurgical phase changes known to occur in carbon steel during rapid cooling.

SYSWELD [12] is a powerful nonlinear finite element code, which not only can be used to analyze temperatures, strains, and stress, but also metallurgical phase changes during welding [6, 13]. In theory, any nonlinear finite element program would be suitable for the simulation of fusion welding. However, SYSWELD has many specialized features and tools that greatly simplify the creation of an accurate welding model. For example, various moving heat source models that accurately represent the heat flux

distribution directly under the welding torch are automatically available in SYSWELD and do not need to be created from scratch.

. In this study, residual stress results for different fillet geometries are compared with previous welding simulation results obtained for a simple “straight” fillet weld in a longitudinal stiffener [12] (see Fig. 1a). In [12], an axisymmetric model was developed to approximate the welding stresses in a circular arc around the end of the longitudinal stiffener. As shown in Fig. 1b, a cross-section of the end of the longitudinal stiffener provides the geometric dimensions for a circular swept arc that can reasonably represent the 3-D state of stress at the far ends of the welded joint. The results in [12] illustrated how the boundary conditions (clamps conditions) and metallurgical phase changes could the influence residual stresses near the fillet weld.

(a)

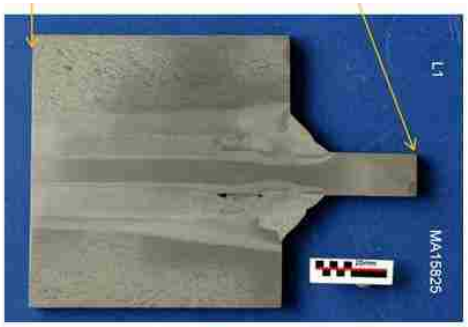

(b)

Figure 1 (a) Longitudinal Stiffeners [3]
(b) Cross-Section View of Longitudinal Stiffeners [6]

The study in [12] demonstrated that very high residual stresses could be expected at the toe of the fillet weld, primarily due to the stress concentration that occurs at this point. However, the study in [12] only examined 45 ° fillet welds (see Fig. 2b), i.e., the angle between the fillet weld and the base bar is fixed at 45 °. It is to be expected that the geometry of the fillet weld, and in particular the contact angle at the weld toe, plays a critical role in the local residual stresses. In an effort to better understand how the stress concentration effect at the weld toe is related to the fillet contact angle, fillet weld geometries were created that examined two extremes: 1) a contact angle of 0 ° (Fig. 2a), and 2) a contact angle of 90 ° (Fig. 2c). The 0 ° fillet weld results in a smooth weld toe that is tangent to the substrate at the contact point, while the 90 ° fillet model results in an abrupt 90 ° transition from the fillet weld to the substrate.

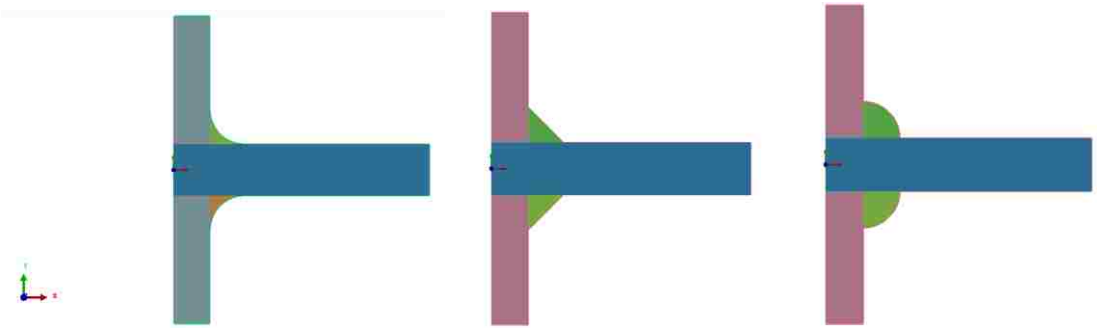

(a) (b) (c)

Figure 2 (a) Tangent (0 °) Fillet Model. (b) 45 ° Fillet Model. (c) 90 ° Fillet Model

Obviously, the fillet welds in these three models differ not only in terms of the edge contact angle, but also have different volumetric shapes. Of greatest interest in the results, are the localized stress concentrations at the toe of the weld, which depend most strongly on the contact angle. The stress concentration effect is very localized and thus it is important to verify that the finite element mesh is sufficiently refined at the weld toe to

accurately capture the stresses at this location. Six models, with different mesh quality, were created to evaluate how the mesh quality and density influenced the accuracy of the stress results for the different welding fillet geometries. As will be shown in the results section, a zone within 1mm of the weld toe must be sufficiently refined to accurately characterize the localized stress concentration effect. Our prediction is that a model with smaller contact angle has a smaller residual stress near the weld toe and results of the model with better mesh quality are more accurate.

Chapter 2

Welding Process Simulation Models

Two different steel alloys were used in this study: 316L austenitic stainless steel and S355J2G3 carbon steel. These two materials were chosen to contrast the residual stresses obtained from a material without metallurgical phase transformation induced stresses (316L) and a material with phase change stresses (S355J2G3).

All three geometric fillet weld models have an initial weld on the top surface (1st welding line), which begins at t=0s, and a 2nd weld (bottom welding line) that is deposited at t=600s. . Those models are constrained on the horizontal plane of symmetry until 4200s when the model has completely cooled down, after which the vertical restraint is released. The welding speed is specified to be 6.329mm/s. The welding width is 12mm and welding penetration is 6 mm. (The energy per unit length is 20J/mm).

To contrast the nature of the welding residual stresses obtained with clamping to the residual stress state without clamping, a sequence of simulations were performed where the model has same setting except that it is entirely unrestrained during welding from 0s (initiation of top weld), , until the structure has completely cooled down to ambient temperature at 4200s. The finite element mesh for the 45 ° and 90 ° fillet weld models were created using SYSWELD's built-in Topo Mesh capability. However, creation of the 0 ° fillet weld, or tangent model, results in a very thin zone near in the neighborhood of the weld toe. In order to achieving accurate results, the mesh needs to be very refined near the weld toe and SYSWELD's Topo Mesh capability was unable to

provide a suitable mesh. HYPERMESH [14] was used to create a refined mesh for the 0 ° tangent fillet weld model. Figure 3 depicts meshed models for the three geometric models of interest in this study. In particular, Figs. 3d and 3g show close up views of the narrow mesh obtained using HYPERMESH for the 0 ° tangent fillet weld model. The yellow point in Fig 3 (g) is the tangent point. The tangent fillet model contains 65621 nodes with 23892 quadratic elements (mid-side nodes); the 45 ° fillet model has 25337 nodes and 8864 quadratic elements; the 90 ° fillet model has 40891 nodes and 13990 quadratic elements.

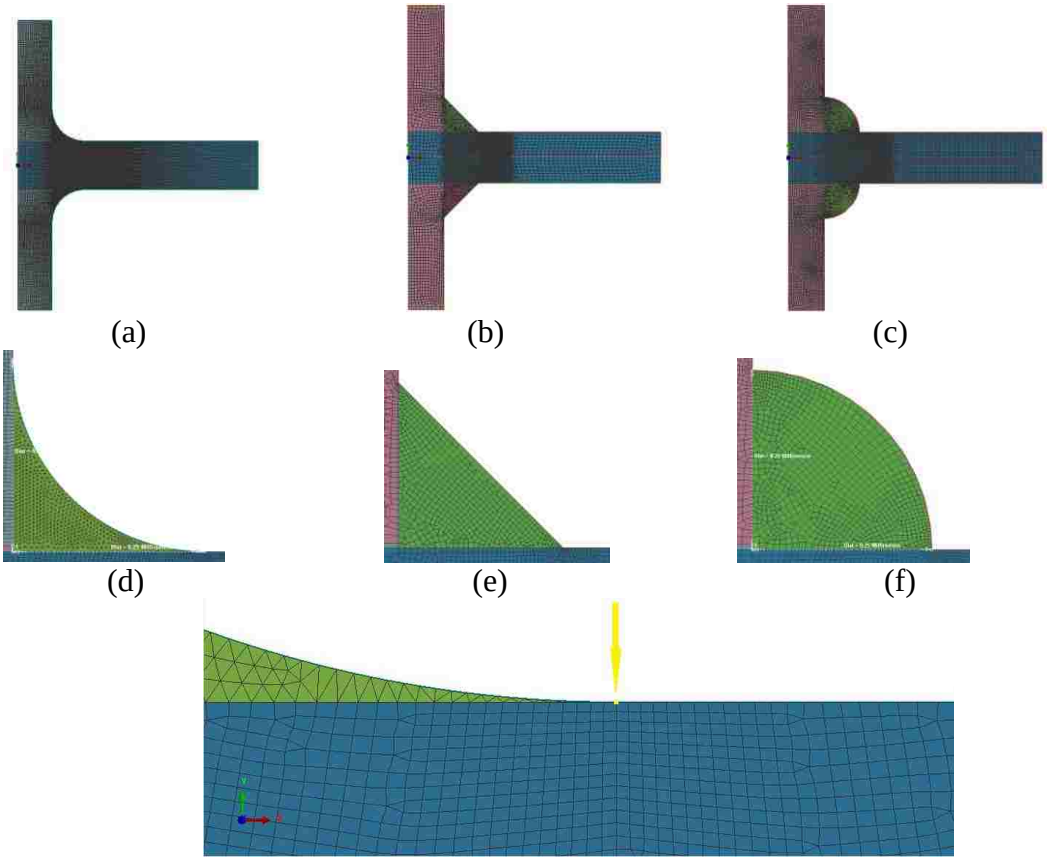

Figure 3 (a) Mesh Model with Tangent Fillet.
(b) Mesh Model with 45 °Fillet. (c)Mesh Model with 90 °Fillet.
(d) Close-Up View of Top Fillet of Tangent Fillet Model.
(e) Close-Up View of Top Fillet of 45 °Fillet Model.
(f) Close-Up View of Top Fillet of 90 °Fillet Model.
(g) Close-Up View of Tangent Fillet Model Close to the Weld Toe.

Chapter 3

Simulation Results

3.1 Heat Transfer Results

The temperature distribution at t=5s after initiation of the 1st weld pass on the upper surface and t=605s (5s after the start of the 2nd, bottom weld) is depicted in Figs. 4 and 5, for the different weld configurations. It should be noted that metal on the lower weld volume is not introduced into the simulation until the bottom weld pass begins at t=600s. Thus, there is a slight difference in the temperature contours between the two (upper and lower) weld passes. In addition, the axisymmetric model shows a temperature concentration towards the axis of rotational symmetry that is not observed in a corresponding 2-D welding simulation. From these results we can find that the HAZ occurs horizontally more than vertically. However, the high temperature zone given by red and pink in the contour plots are increase in size as the contact angle become larger. This is because the larger contact angle model has more energy input because of its bigger volume. If I changed the welding parameter in order to make them have same energy input, temperature distribution is similar and tangent fillet model has highest peak temperature （ because of smallest volume (Figs 4(d)-(e), 5(d)-(e)).

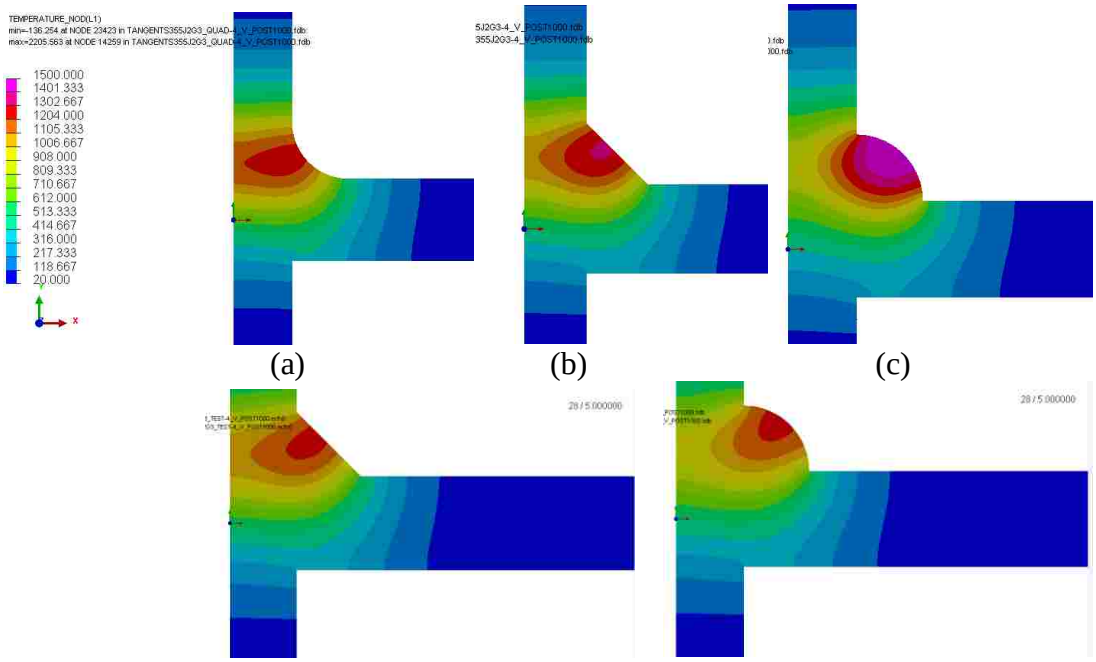

(a) (b) (c)

(d) (e)

Figure 4 Temperature Distribution at t=5s.

(a) Tangent Fillet Model. (b) 45 °Fillet Model. (c) 90 °Fillet Model.
(d) 45 °Fillet Model with same energy input as Tangent Fillet Model.
(e) 90 °Fillet Model with same energy input as Tangent Fillet Model.

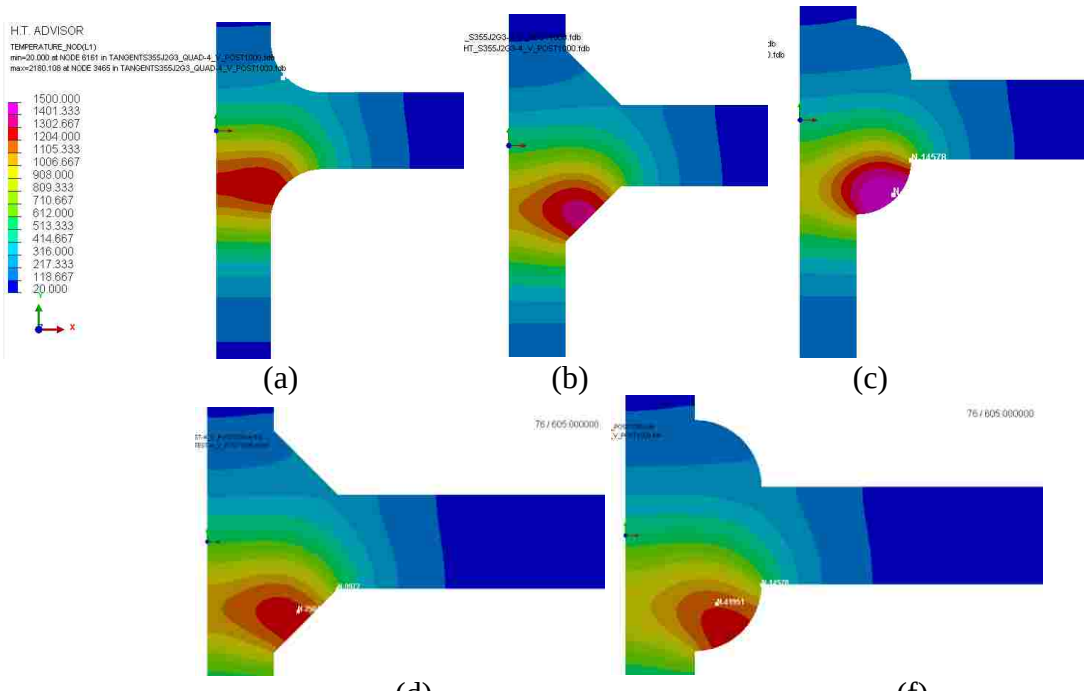

(a) (b) (c)

(d) (f)

Figure 5 Temperature Distribution at t=605s.

(a) Tangent Fillet Model. (b) 45 °Fillet Model. (c) 90 °Fillet Model.
(d) 45 °Fillet Model with same energy input as Tangent Fillet Model.
(e) 90 °Fillet Model with same energy input as Tangent Fillet Model.

The plots in Fig. 6 show the transient temperature distribution along the top and bottom surfaces. The temperature is always smaller for the fillet weld with smallest contact angle The 90° model temperature reaches 850℃ on the weld toe of the top surface and the tangent model temperature only reaches 500℃ on the top surface at weld toe because of the smaller energy input at t=5s. Similar situation happened on bottom surface. After the distance from weld toe increases to 15mm, the temperature in these three different models on both the top surface and bottom surface are almost the same.

Different temperature distribution would cause different residual stress distribution for these models, especially for S355J2G3 material, which undergoes metallurgical phase transformations during cooling.

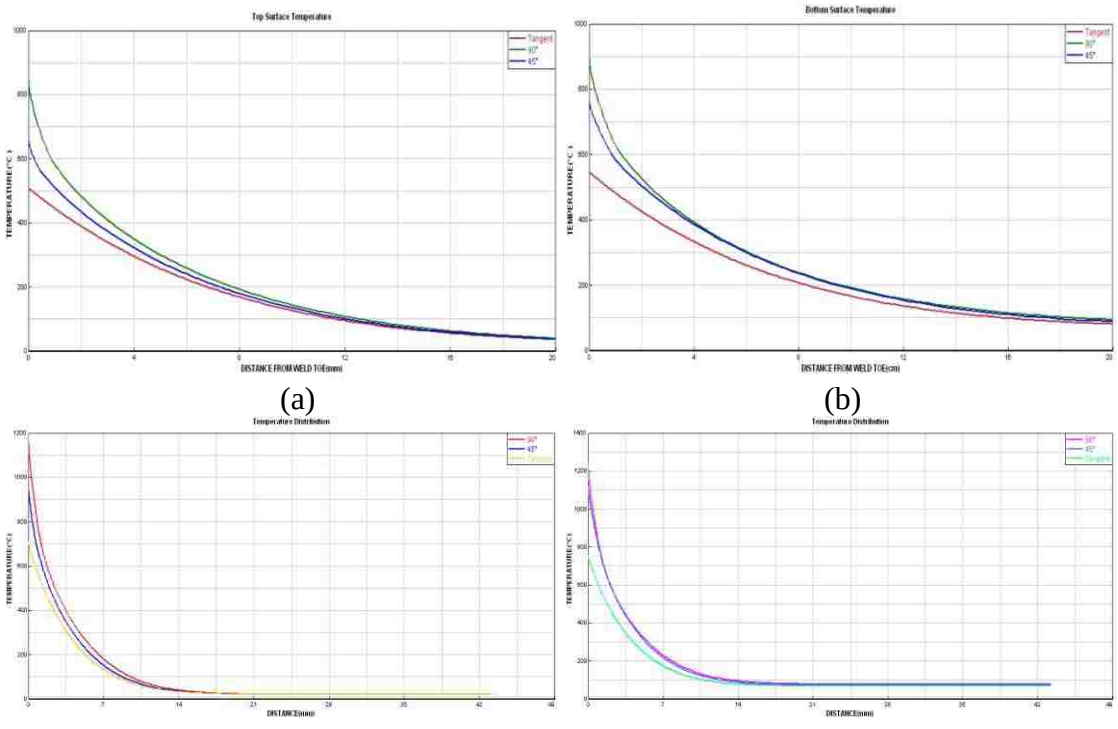

(a) (b)

(c) (d)

Figure 6 Temperature Distribution Measured from Weld Toe
(a) Top Surface Temperature Distribution at t=5s.
（b）Bottom Surface Temperature Distribution at t=605.
(c) Top Surface Temperature Distribution at t=2s.
(d) Bottom Surface Temperature Distribution at t=602.

3.2 Results of Residual Stresses in 316L Stainless Steel

No surprisingly, the σ_{xx} stress results show that there is a stress concentration near the welding toe at t=4201s after releasing the clamp conditions at t=4200s. Figure 7 shows that the σ_{xx} stress distributions for the tangent model, 45 ° model, and 90 ° model. As can be seen, all three welding models have similar σ_{xx} stress distribution. It should be noted that the stresses are not perfectly symmetric, since the lower weld fillet does not exist when upper weld is deposited. Thus, not only is the temperature asymmetric, but the final residual stress distribution is a combination of the residual stresses that result arise from the 1st and 2nd weld passes.

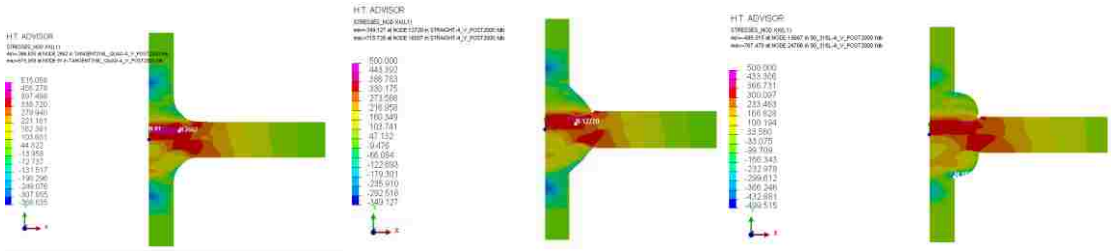

(a) (b) (c)

Figure 7 Residual Stress σ_{xx} Distribution at t=4201s after Releasing Clamp
(a) Tangent Model. (b) 45 ° Model. (c) 90 ° Model.

The plot of σ_{xx} on top surface (Fig. 8), measured from the weld toe shows that within 2mm of the weld toe, the σ_{xx} stress obtained from the 45 ° model and 90 ° model increase more rapidly as one approaches the weld toe and reaches about 700MPa on the weld toe. The difference of those σ_{xx} curves is the curve of σ_{xx} stress of 90 ° model is steeper. However the σ_{xx} stress obtained from the tangent model exhibits a linear behavior and only reaches a magnitude of 360MPa at the weld toe. These results are easy to be explained: a none-zero contact angle could cause a stress concentration near to the contact position because of geometric discontinuities [15]. The σ_{xx} stress component in all

three curves shown in Fig. 8 (a), (b) suddenly decreases when extremely close to the weld toe, but these results may not be considered correct. Because of the boundary condition may not be satisfied near the weld toe where the geometry changed.

However, Figure 8(b) illustrates an unexpected result, i.e., the σ_{xx} stresses from the tangent model are greater in magnitude than the same stress components obtained from the other two models. Unlike Figure 8(a), the curve of 90 °model reaches lower than curves of 45 °model and tangent model at the welding toe.

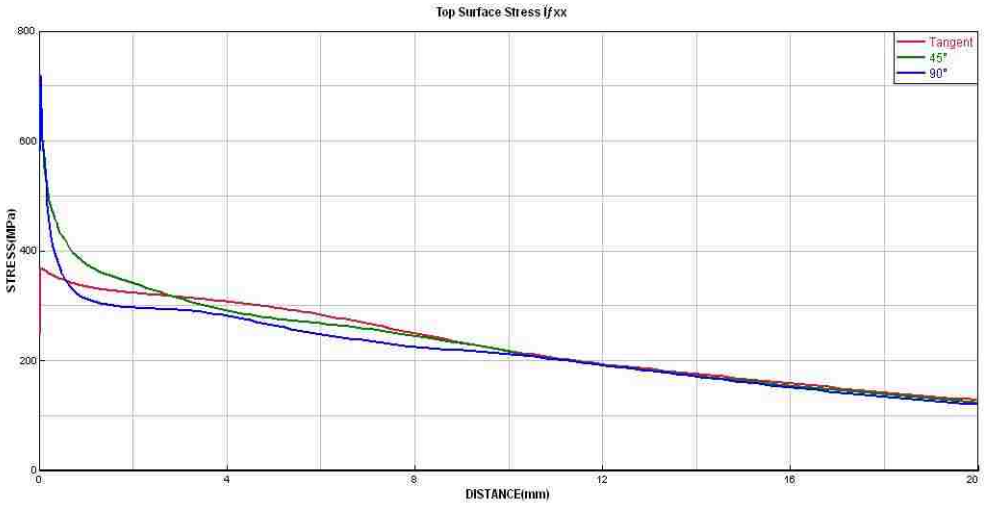

(a)

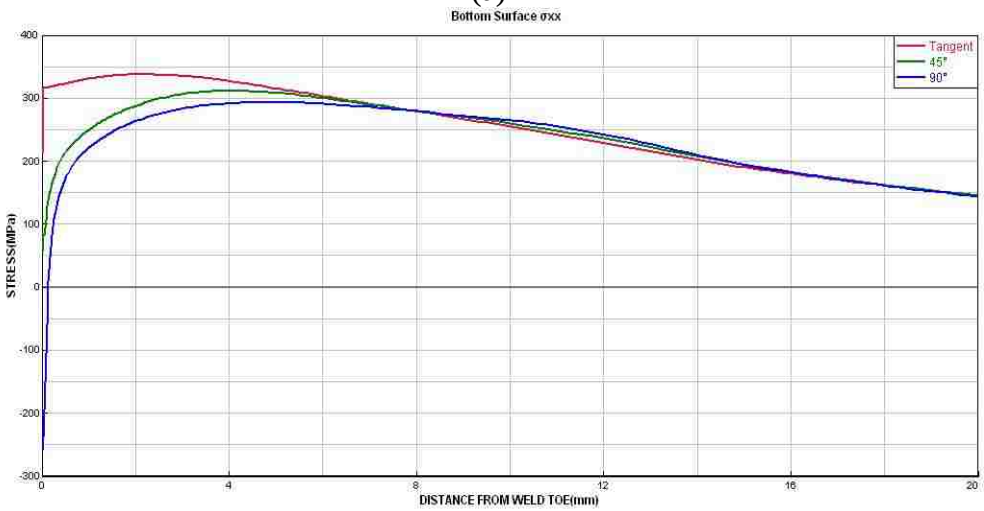

(b)

Figure 8 Residual Stress σ_{xx} Distribution at t=4201s after Releasing Clamp (a) Top Surface Results. (b) Bottom Surface Results.

Because the magnificent σ_{xx} stresses change when close to the weld toe, it is necessary to check the validity of these results. Boundary condition may be failure when near to the welding toe. On the top surface and bottom surface, which are free surface, σ_{yy} and σ_{xy} stresses should be zero. We can use σ_{yy} and σ_{xy} to check if those results are reliable. From figure 9 (a) we know that σ_{yy} and σ_{xy} stresses obtained from the tangent model is zero in all position along top and bottom path, it means the results of tangent model is accurate on the top and bottom surface even very close to the weld toe. Figure 9 (b) and (c) shows σ_{xx} stress results of $45°$ model and $90°$ model are correct with the distance to welding toe larger than 0.06mm and 0.08mm.

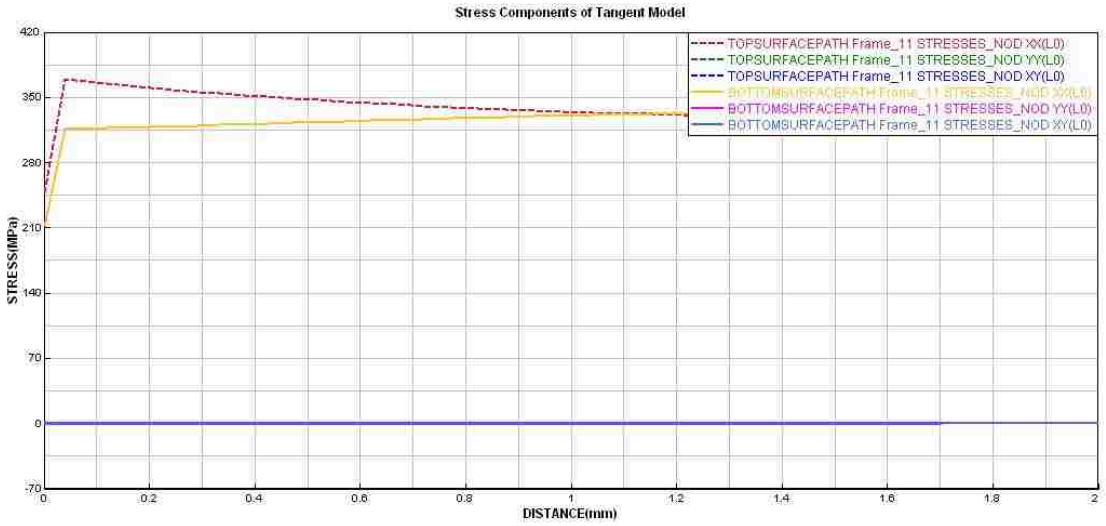

(a)

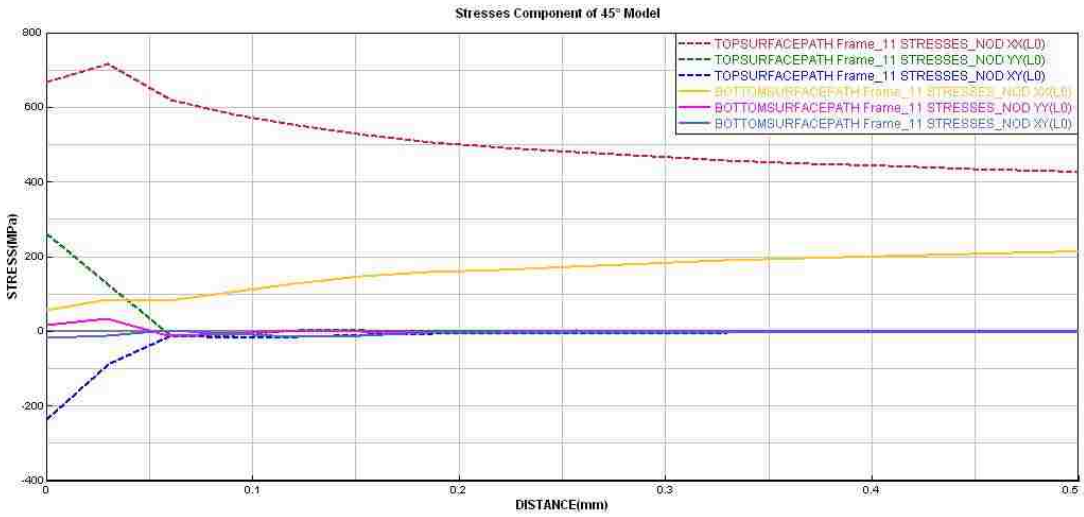

(b)

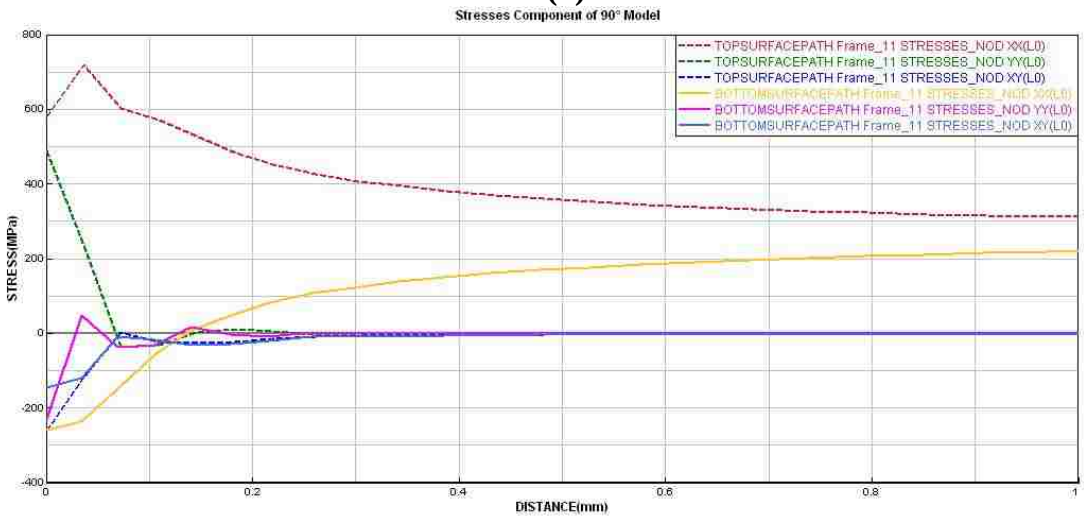

(c)

Figure 9 Stress Components σ_{xx}, σ_{xy}, σ_{yy} on Top and Bottom Surface Measured from welding toe. (a) Stress Components of Tangent Model.
(b) Stress Components of 45 °Model. (c) Stress Components of 90 °Model.

Now, let's show the σ_{xx} stress within 2mm from welding toe. The unreliable results zones are marked by gray. We find that σ_{xx} stress of top and bottom surface of tangent model are similar and 45 ° model have a much smaller σ_{xx} Stress on bottom surface difference. 90 ° model even has a larger σ_{xx} Stress difference between top surface and bottom surface.

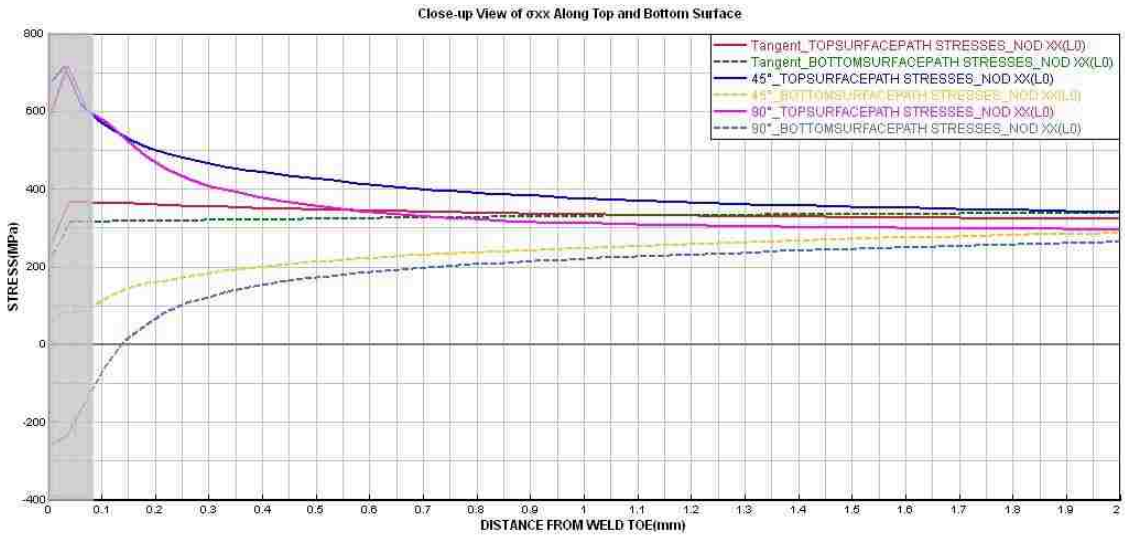

Figure 10 Close-up View of σ_{xx} stress along top and bottom surface at t=4201s.

If we compare results at t=4200s (clamped conditions), we find that σ_{xx} stresses in all of the models is reversed between bottom and top surface. This stress reversal is explained in [6]. The reason: spring back and bending occurs after releasing the clamp, resulting in an un-axisymmetric stress distribution. Basically, σ_{xx} stresses of 45° model and 90° model are larger than the stresses obtained from the tangent model at 0.08mm from weld toe. The 90° model and 45° model have almost the same σ_{xx} stress on bottom surface path and their curves look like the curves for the σ_{xx} stress component from the 90° model and 45° models on the top surface at t=4201s. These are the expected results. However, after releasing clamp, the difference in the σ_{xx} stress between top surface and bottom surface increased. Measured from 0.08mm away from the weld toe , that difference of σ_{xx} stress of 45° model and 90° model has increased from 100MPa, 200MPa to 500MPa and 700MPa. Only the tangent model keeps the same σ_{xx} stress difference. Figure 12 shows σ_{xx} stresses measured from the bottom weld toe to the top welding toe through the cross-section of the horizontal bar. It indicates that the weld fillet geometry

influence the stress reversal after releasing the clamp. A bigger plate contact angle would cause a larger stress difference between top and bottom surface with clamp. As a result, it's anticipated that a larger contact angle would cause a larger stress change after releasing clamp.

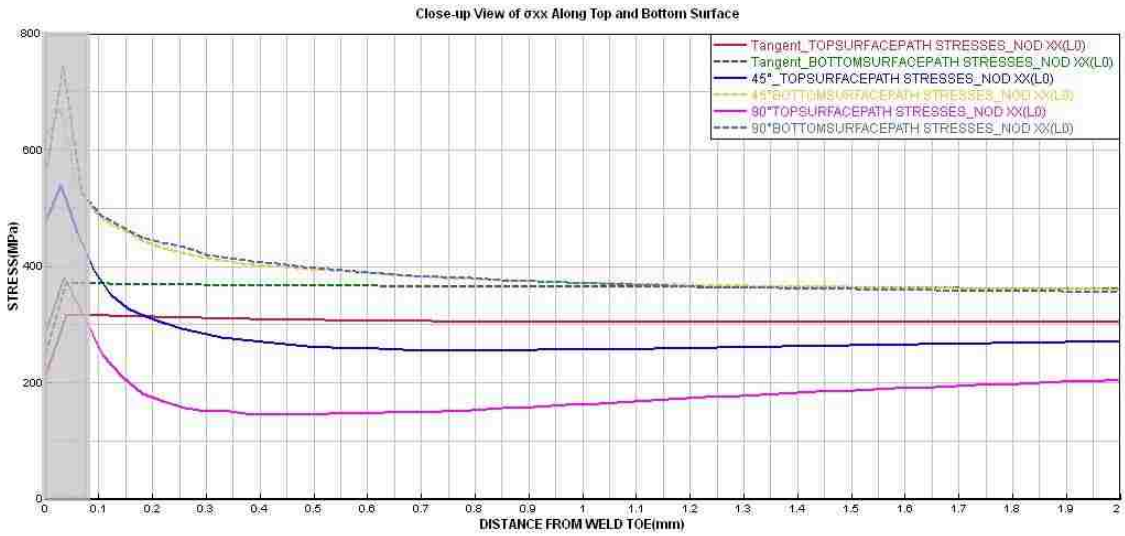

Figure 11 Close-up View of σ_{xx} stress along top and bottom surface at t=4200s.

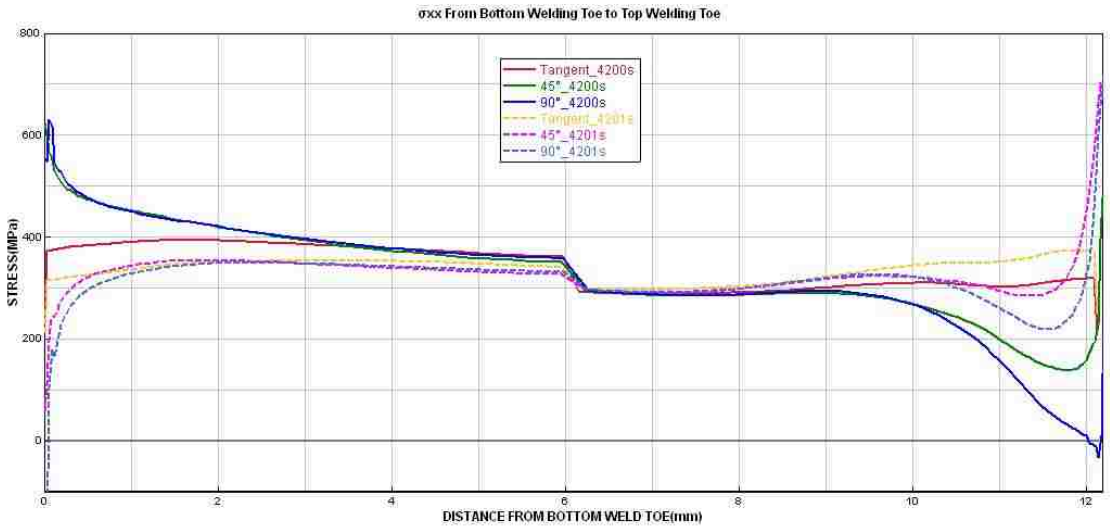

Figure 12 σ_{xx} Stresses Measured From Bottom Welding Toe to Top Welding Toe at t=4200s with Clamp and t=4201s after Releasing Clamp.

The same welding simulations performed without any clamping restraints results in very different residual stresses. The computed σ_{xx} stresses in this case, given on the

surface from the weld toe at t=4201s, is shown in Figure 13. We noticed that top surface and bottom surface have a similar σ_{xx} stress distribution for this model, and the σ_{xx} stress on the bottom surface is always lower than top surface. The tangent model has the lowest σ_{xx} stress curves, with no apparent stress concentration. The 90 ° model has the highest σ_{xx} stress values. Both the 90 ° model and 45 ° model have higher stresses close to the weld toe and display a stress concentration. These result completely fit our prediction which tangent model has a lower residual stress near the weld toe.

A simulation which all three models have same energy input was also be build and its results are almost the same as those results above. It means residual stresses are not sensitive to energy input for 316L stainless steel without metallurgical phase transformation.

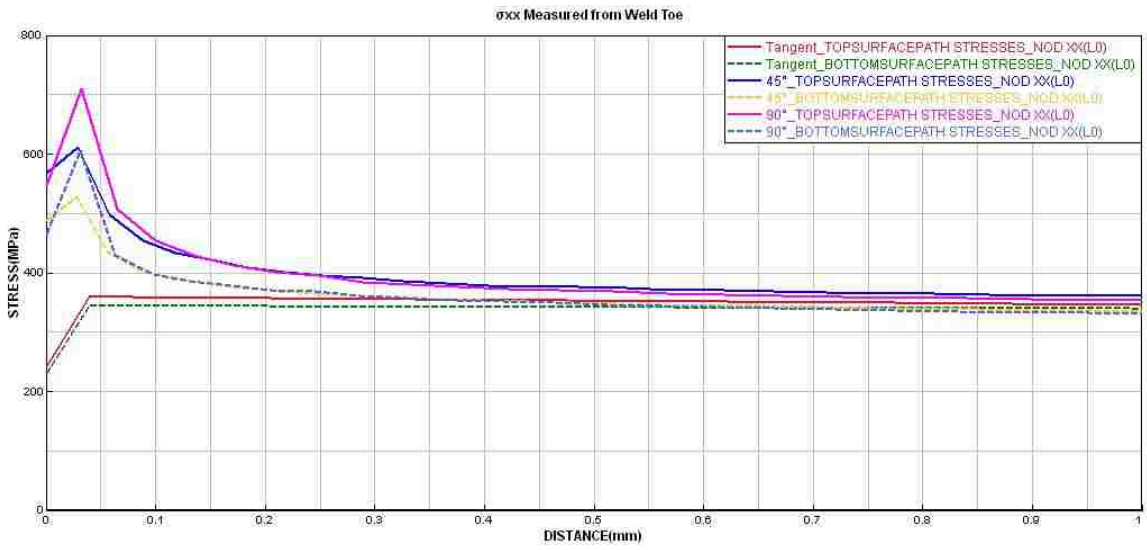

Figure 13 σ_{xx} Stresses Measured from Weld Toe at t=4201s with No Clamp

3.3 Results of Residual Stresses in S355J2G3

Results of S355J2G3 are more complex than 316L stainless steel. Because the metallurgical phase changes can affect the magnitude of the residual stresses. When

carbon steels are heated above the eutectoid temperature, the pearlite or austenite-martensite will transform to austenite, and the austenite will transform to pearlite, bainite and martensite during cooling [6]. Pearlite, bainite and martensite have different physical properties and will change the residual stresses due to localized volumetric strains.

3.3.1 Results with Different Energy Input

Because of different weld fillet volume, the energy input for these models are different. Figure 14 shows the σ_{xx} stress distribution in the S355J2G3 material models. It is much different than the results given in Figure 7 at the same time for the 316L stainless steel. The S355J2G3 models also bend and change the stress distribution after releasing clamp in a manner similar to the 316L models.

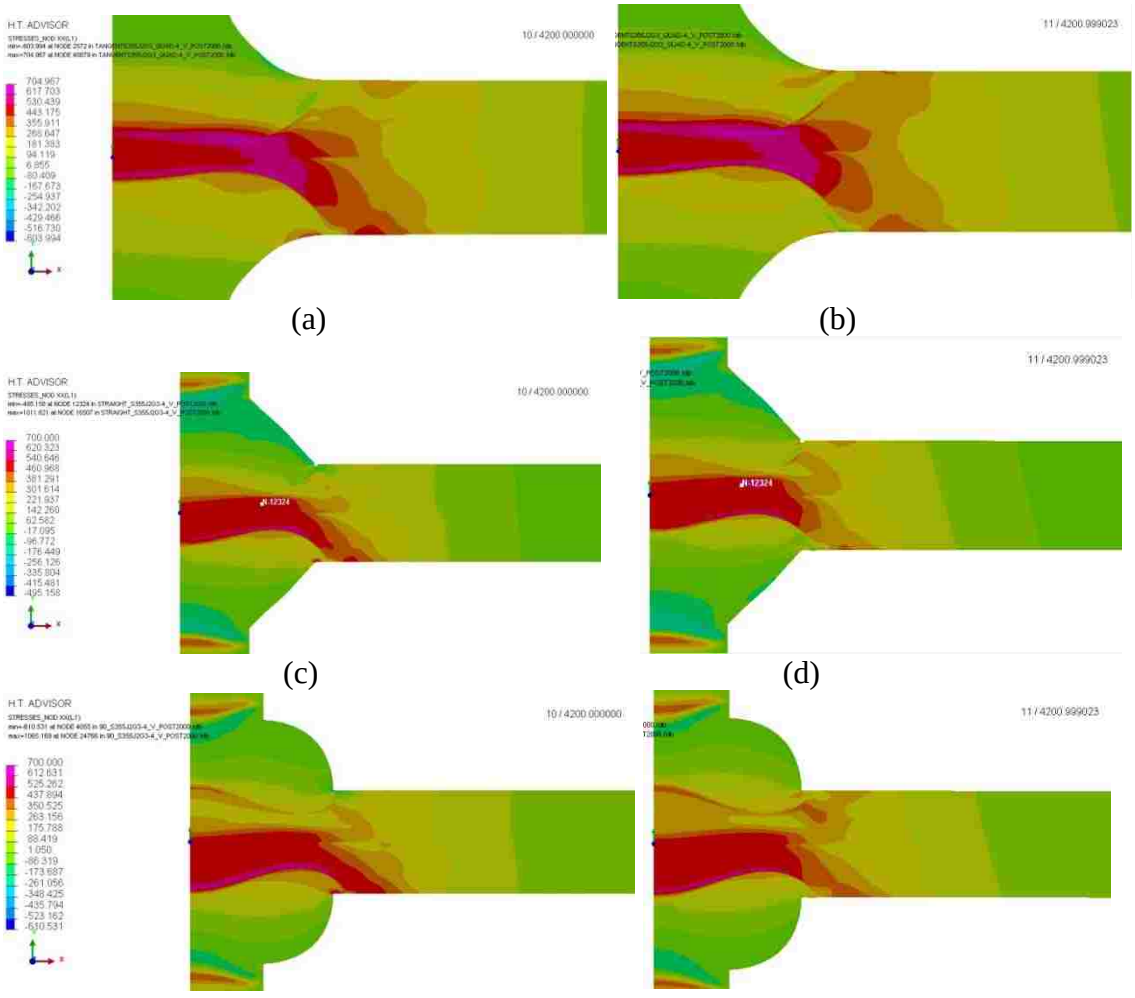

(e) (f)

Figure 14 Residual Stress σ_{xx} Distribution (a) Tangent Model with Clamp at t=4200s. (b) Tangent Model after Releasing Clamp at t=4201s. (c) 45 °Model with Clamp at t=4200s. (d) 45 °Model after Releasing Clamp at t=4201s. (e) 90 °Model with Clamp at t=4200s. (f) 90 °Model after Releasing Clamp at t=4201s

As in the previous simulations for 316L, it's important to check the validity of results by examining the normal and shear stress distributions on the surface. Figure 15(a), (b), (c) indicate that the results are correct when the distance measured from weld toe is larger than 0.75mm for the 45 °model and 1.2mm for the 90 °model on top surface. There is a result for the tangent model which indicate its curves are accurate on top surface. Figure 15(d), (e) indicate an interesting result. There are two zones that are invalid for the 45 °model and 90 °model, one is from weld toe to 0.15mm for the 45 °model and 0.3mm for the 90 ° model, the other one is match the rapidly increasing zone when closing to welding toe which is between 0.8mm and 1.4mm.

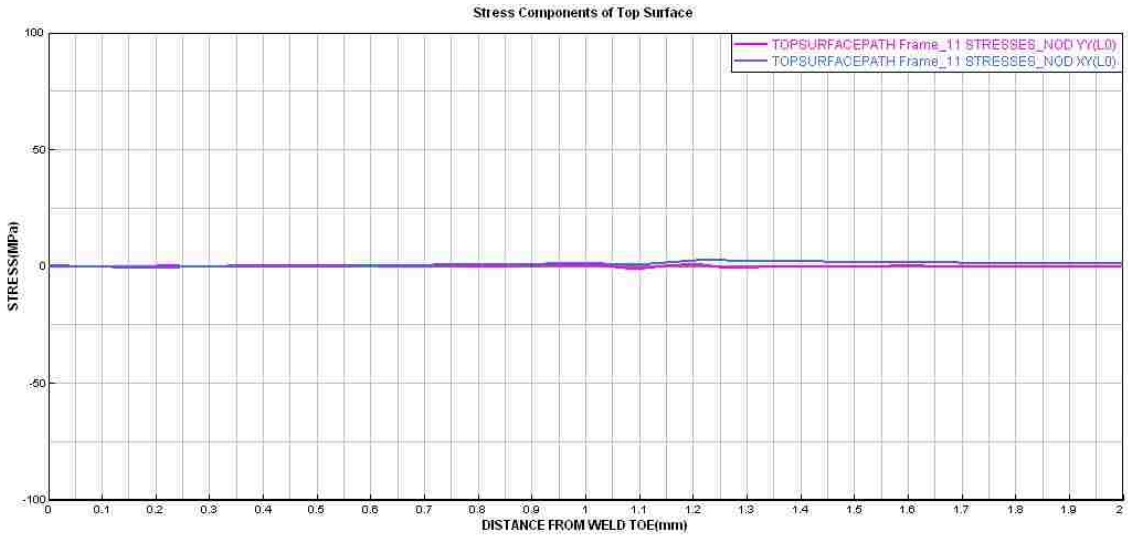

(a)

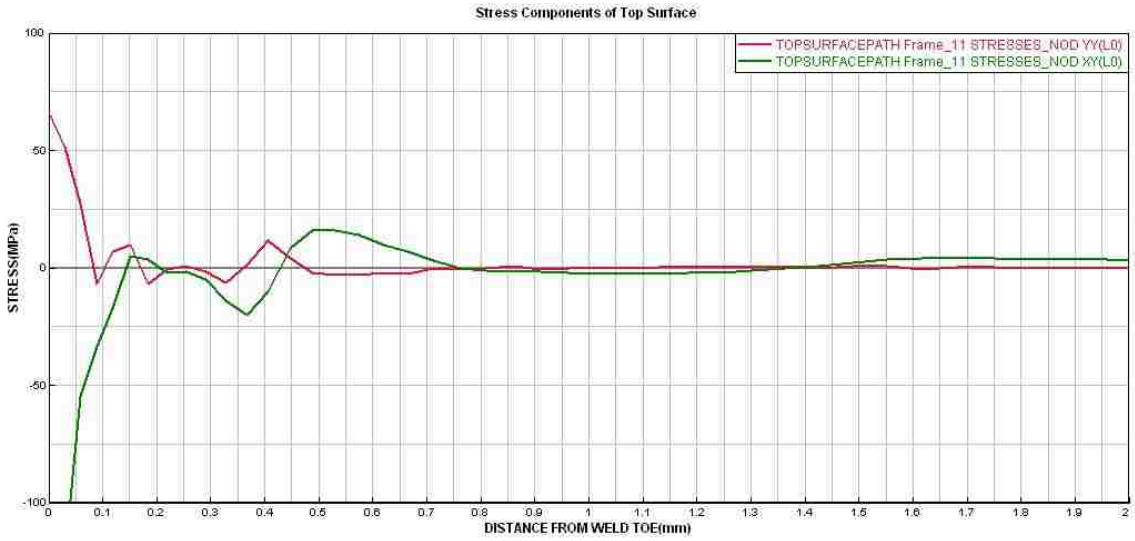
Stress Components of Top Surface
TOPSURFACEPATH Frame_11 STRESSES_NOD YY(L0)
TOPSURFACEPATH Frame_11 STRESSES_NOD XY(L0)
STRESS(MPa)
DISTANCE FROM WELD TOE(mm)

(b)

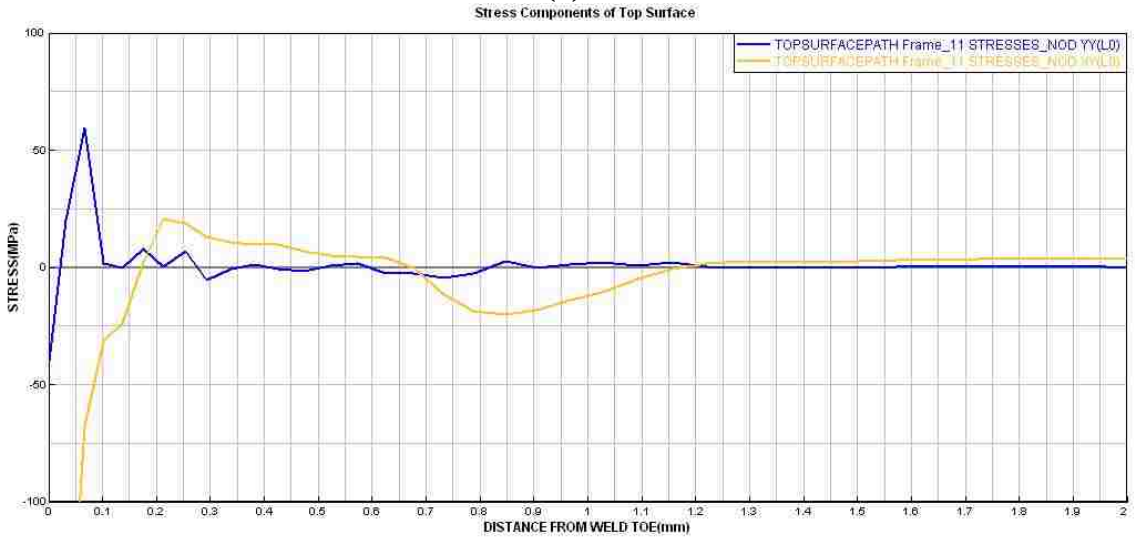
Stress Components of Top Surface
TOPSURFACEPATH Frame_11 STRESSES_NOD YY(L0)
STRESS(MPa)
DISTANCE FROM WELD TOE(mm)

(c)

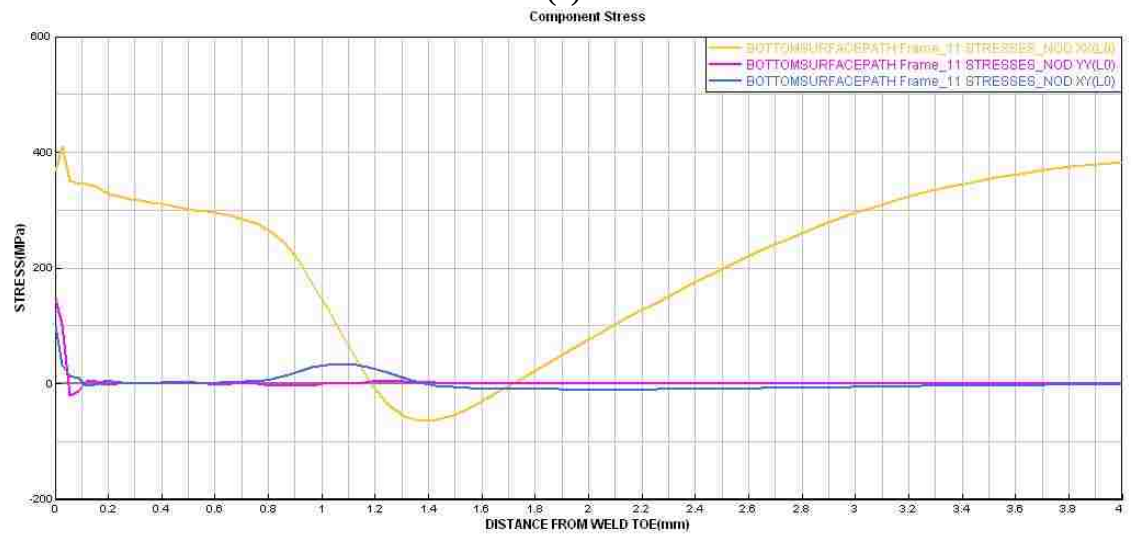
Component Stress
BOTTOMSURFACEPATH Frame_11 STRESSES_NOD YY(L0)
BOTTOMSURFACEPATH Frame_11 STRESSES_NOD XY(L0)
STRESS(MPa)
DISTANCE FROM WELD TOE(mm)

(d)

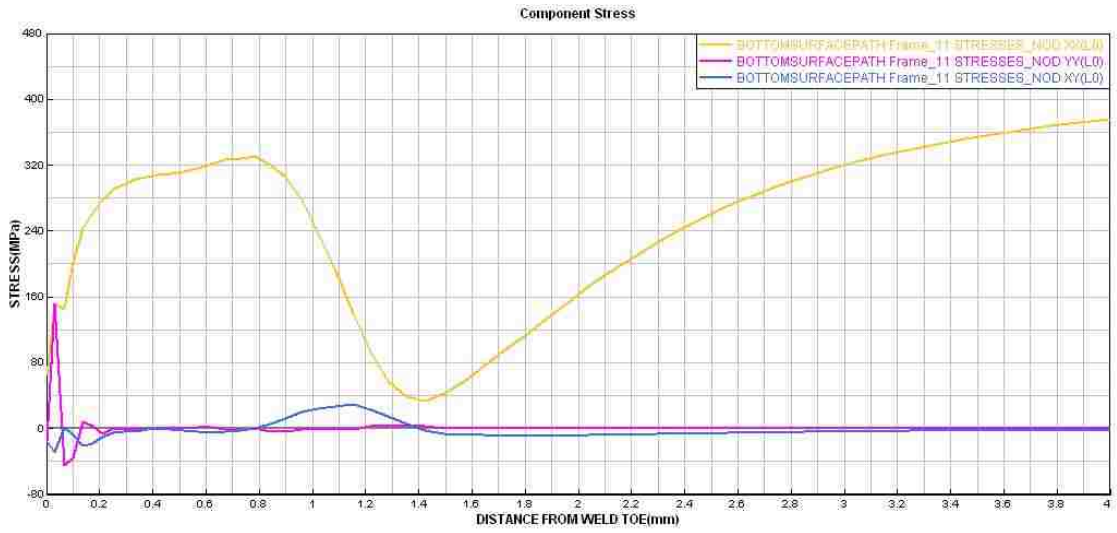

(e)

Figure 15 Stress Component of σ_{xy}, σ_{yy} Measured from Welding Toe
(a) Tangent Model Top Surface. (b) 45 °Model Top Surface. (c) 90 °Model Top Surface.
(d) 45 °Model Bottom Surface. (e) 90 °Model Bottom Surface.

Within validity range, when approaching welding toe, the σ_{xx} stress of top surface of all models increase first then reduce and the σ_{xx} stress of bottom surface of all models increase first then reduce and increase again at last. Unlike the result of 316L stainless steel, on top surface, The tangent top path σ_{xx} stress perform a similar curve as 45 °model and 90 °model top path, just higher. The value of σ_{xx} stress of tangent model is larger than 45 °model and 90 °model is smallest. On bottom surface, all three curves also have similar behavior and almost have same value when the distance to the welding toe is larger than 4.8mm. On bottom surface, the value of σ_{xx} stress of tangent model is larger than 45 °model. Smaller the plate contact angle is, deeper the curve of σ_{xx} stress will reach on bottom surface. Those results indicate that the σ_{xx} stress of tangent is larger than 45 °model and 90 °model with the distance from welding toe between 1.2mm and 4.8mm. However, I guess that on the bottom surface within 1mm of welding toe, the σ_{xx} stress of tangent model is much smaller than other two models. Because the phase change

will reduce residual stress for all models, but geometry change will cause stress concentration near to the welding toe for 45° model and 90° model. That's the reason why the σ_{xx} stress increasing rapidly when approaching welding toe for 45° model and 90° model.

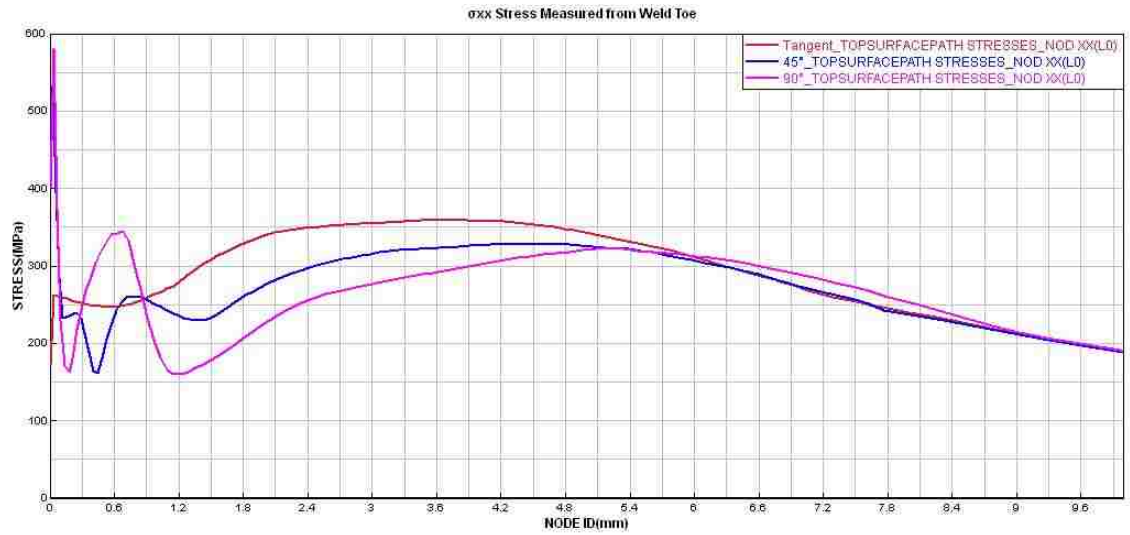

(a)

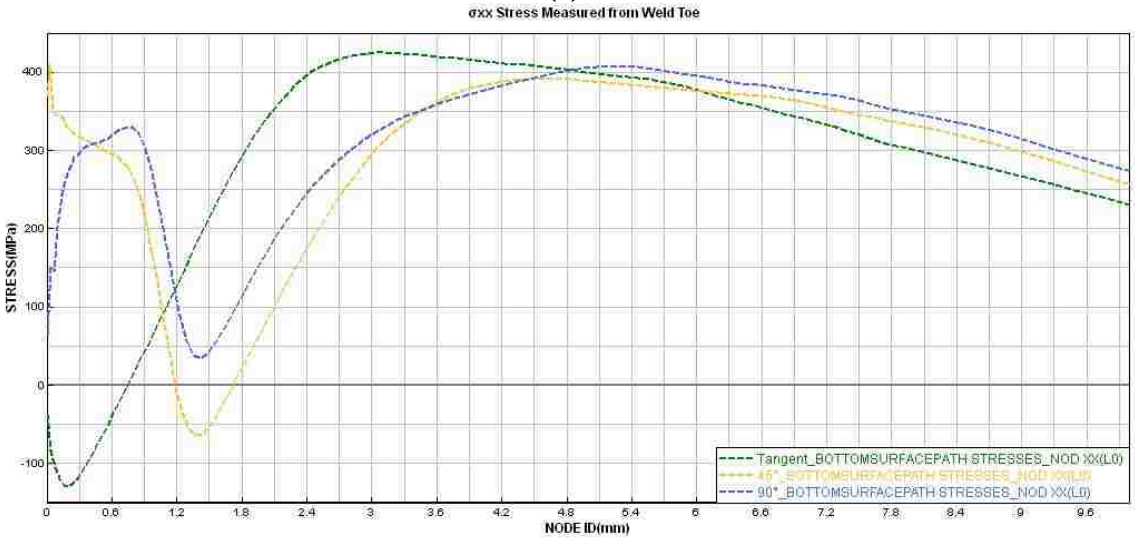

(b)

Figure 16 Residual Stress σ_{xx} Distribution Measured from Weld Toe at t=4201 after releasing clamp.
(a) Top Surface Path. (b) Bottom Surface Path.

If we measured the σ_{xx} stress at t=4200s with clamp to compared with results at t=4201s after releasing clamp. At first sight, these curves of results at t=4200s with clamp looks like similar with those curves at t=4201 after releasing clamp. I pick up several points to compare results at t=4200s with result at t=4201s.

Distance from welding toe is 1.2mm:

	Estimated σ_{xx} Stress of Tangent Model	Estimated σ_{xx} Stress of 45 ° Model	Estimated σ_{xx} Stress of 90 ° Model
Top Surface Path at t=4201s	275 Mpa	230 Mpa	160 Mpa
Top Surface Path at t=4200s	175 Mpa	60 Mpa	-50 Mpa
Top Surface Path σ_{xx} Changed	**100 MPa**	**170 MPa**	**210 MPa**
Bottom Surface Path at t=4201s	125 Mpa	-25 Mpa	125 Mpa
Bottom Surface Path at t=4200s	220 Mpa	180 Mpa	310 Mpa
Bottom Surface Path σ_{xx} Changed	**-95 MPa**	**-205 MPa**	**-185 MPa**

Distance from welding toe is 1.8mm:

	Estimated σ_{xx} Stress of Tangent Model	Estimated σ_{xx} Stress of 45 ° Model	Estimated σ_{xx} Stress of 90 ° Model
Top Surface Path at t=4201s	325 Mpa	260 Mpa	200 Mpa
Top Surface Path at t=4200s	240 Mpa	100 Mpa	20 Mpa
Top Surface Path σ_{xx} Changed	**85 MPa**	**160 MPa**	**180 MPa**
Bottom Surface Path at t=4201s	300 Mpa	25 Mpa	125 Mpa
Bottom Surface Path at t=4200s	390 Mpa	300 Mpa	190 Mpa
Bottom Surface Path σ_{xx} Changed	**-90 MPa**	**-275 MPa**	**-315 MPa**

Distance from welding toe is 3mm:

	Estimated σ_{xx} Stress of Tangent	Estimated σ_{xx} Stress of 45 °	Estimated σ_{xx} Stress of 90 °

	Model	Model	Model
Top Surface Path at t=4201s	355 Mpa	320 Mpa	275 Mpa
Top Surface Path at t=4200s	280 Mpa	180 Mpa	130 Mpa
Top Surface Path σ_{xx} Changed	**75 MPa**	**140 MPa**	**145 MPa**
Bottom Surface Path at t=4201s	425 Mpa	300 Mpa	320Mpa
Bottom Surface Path at t=4200s	500 Mpa	430 Mpa	470 Mpa
Bottom Surface Path σ_{xx} Changed	**-75 MPa**	**-130 MPa**	**-150 MPa**

From these results above, we know that all these S355J2G3 models also bend after releasing clamp and reverse the σ_{xx} Stress of top and bottom surface. But the stress is changed smaller than 316L stainless steel models after releasing clamp. Fillet geometry also affects the stress reverse after releasing clamp. Smaller plate contact angle, smaller stress change after releasing clamp.

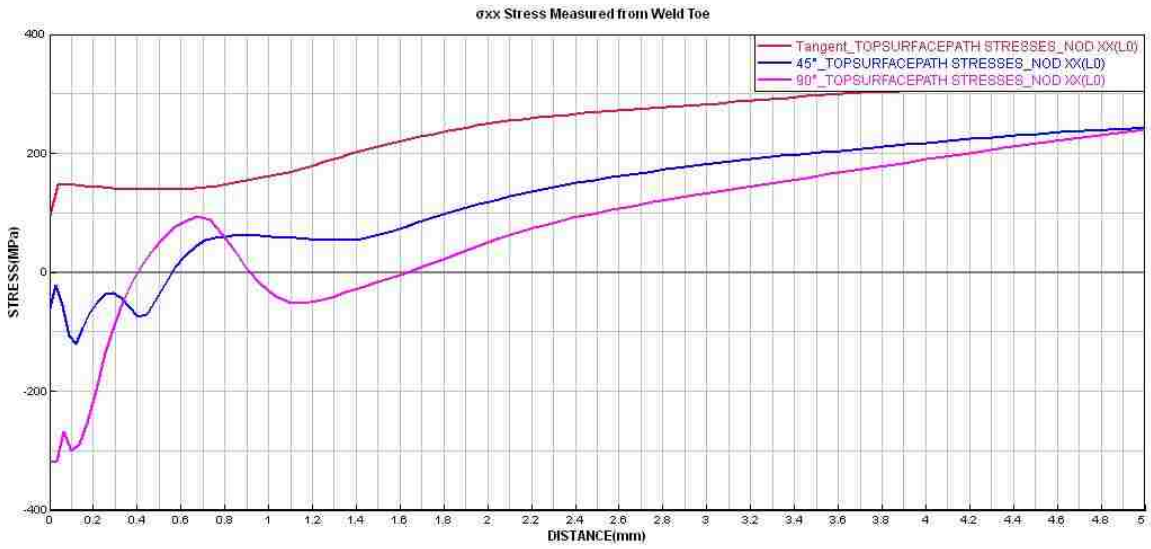

(a)

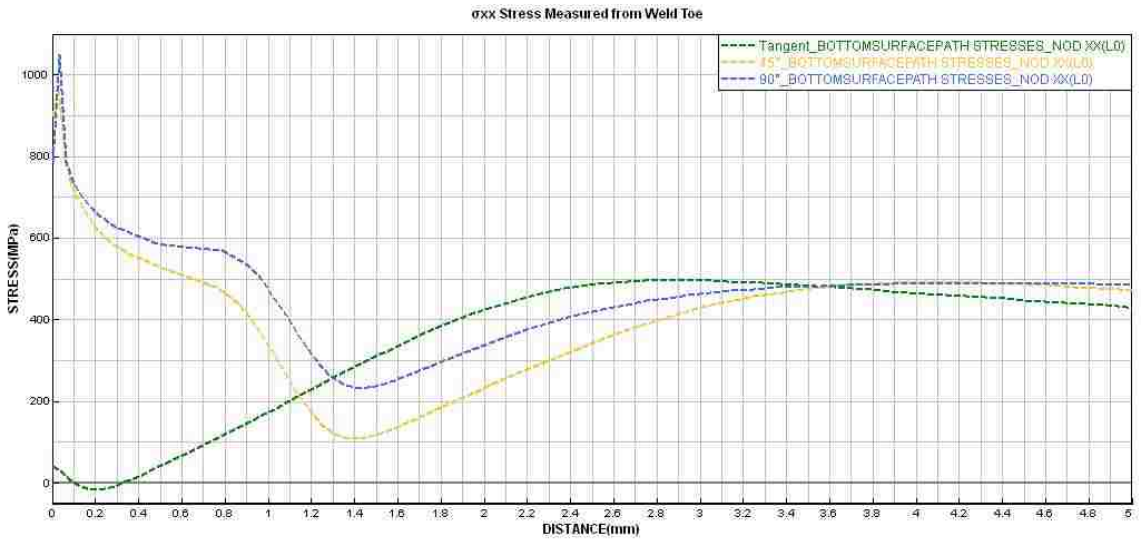

(b)

Figure 17 Residual Stress σ_{xx} Distribution Measured from Weld Toe at t=4200s with Clamp.

(a) Top Surface Path. (b) Bottom Surface Path.

Those results above show no matter at t=4200s with clamp or at t=4201s after releasing clamp, the σ_{xx} Stress of tangent model is always larger than other two models in most part of surface. It is not our expectation. Considering results of phase change, we find that different fillet geometry will cause different metallurgical phases distribution because of smaller fillet volume has smaller energy input in this simulation. It will cause different residual stress. Phase change could cause reducing of residual stress and Figure 18(j) shows tangent model has least phase change along top surface path and 90° model has most. Comparing figure 16(a) with figure 10, we find the residue stress of tangent model on top surface reduces less than other two models. As a result, the σ_{xx} Stress of tangent model is largest on top surface generally. But on bottom surface, a smaller plate contact angle model would reduce σ_{xx} to a smaller value even less than zero when approaching to welding toe.

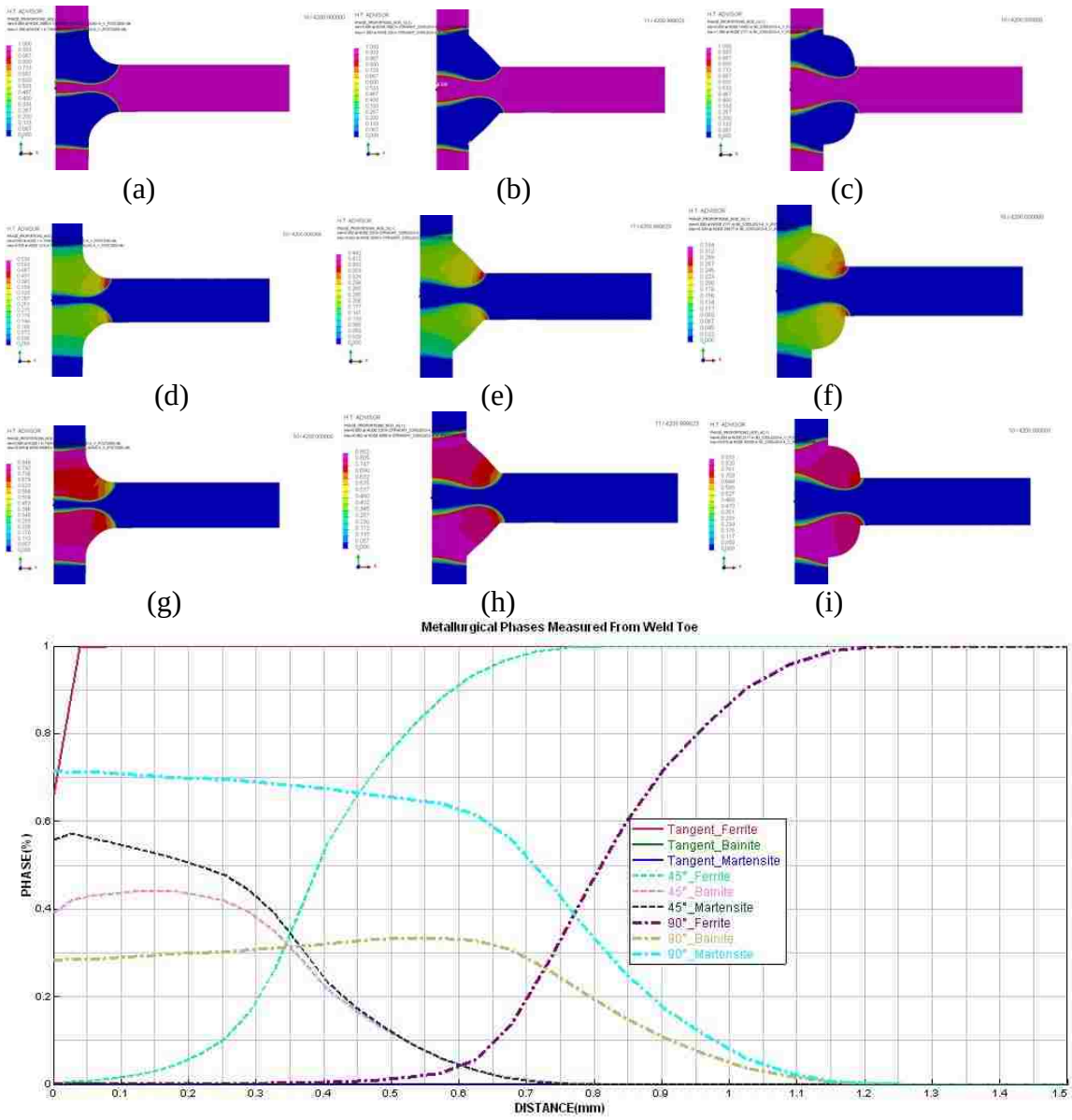

Figure 18 Metallurgical Phases in S355J2G3 at t=4201s.
(a) Ferrite of Tangent Model. (b) Ferrite of 45 °Model. (c) Ferrite of 90 °Model.
(d) Bainite of Tangent Model. (e) Bainite of 45 °Model. (f) Bainite of 90 °Model.
(g) Martensite of Tangent Model. (h) Martensite of 45 °Model.
(i) Martensite of 90 °Model.
(j) Metallurgical Phases Percentage of Three Models on Top Surface Measured from Weld Toe

With no clamp, Stress σ_{xx} of these three models are almost the same within validity range on top surface. On bottom surface, results of 45 °Model and 90 °Model are

also almost the same, but the curve of tangent model is higher than other's. Those results on bottom surface with no clamp is similar to results on bottom surface with clamp at t=4201s. From those results we also see the tangent model is less sensitive to clamp condition than other two models. In both no clamp and clamp situation, In 316L stainless steel tangent model, σ_{xx} stress on top surface and bottom surface are similar, but in S355J2G3 tangent model they are much different. It could be caused by un-axisymmetric phase change.

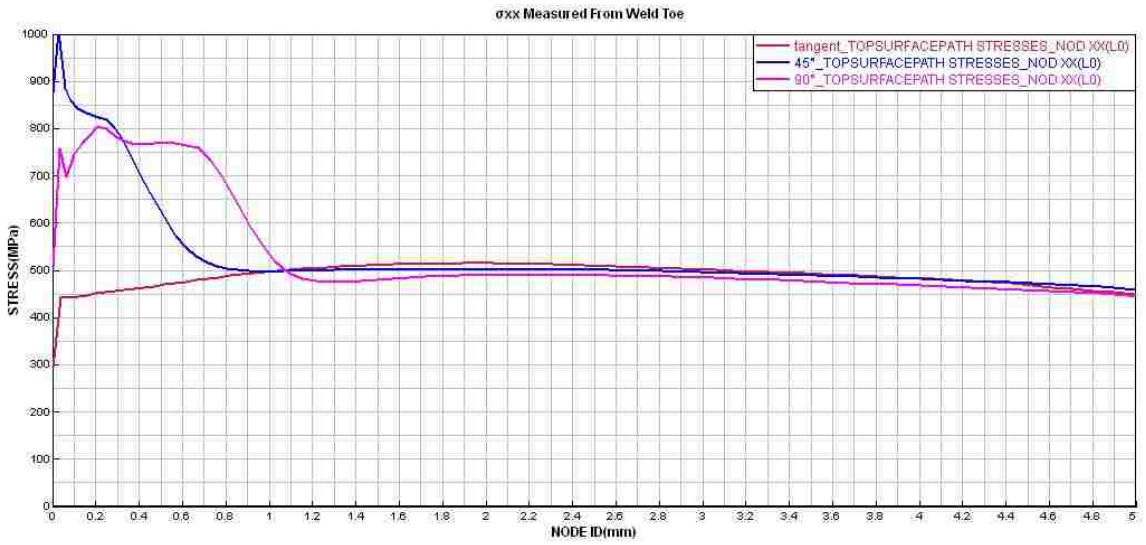

(a)

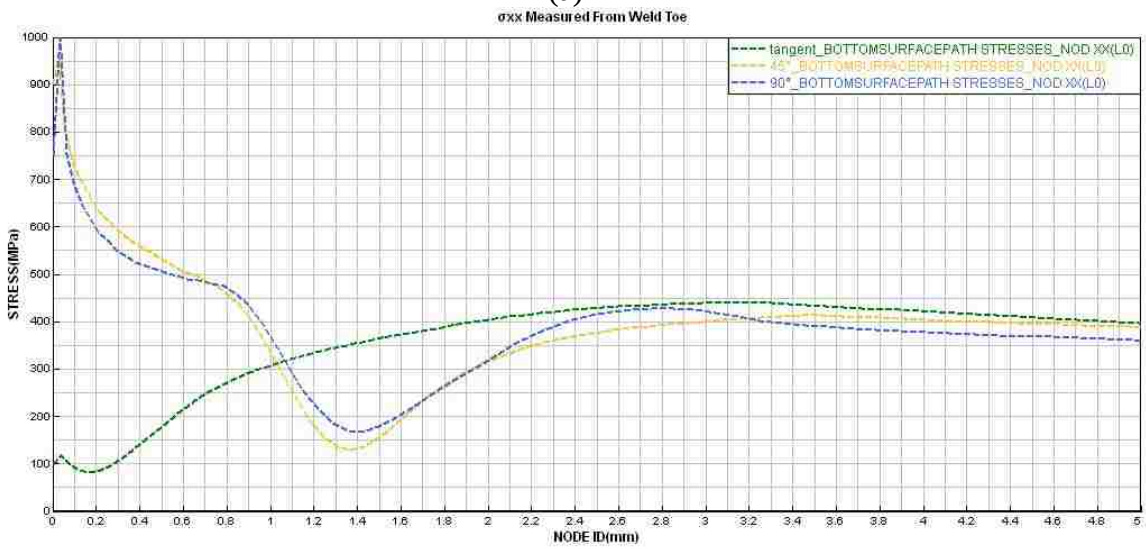

(b)

Figure 19 Residual Stress σ_{xx} Distribution Measured from Weld Toe at t=4201s with No

Clamp.
(a) Top Surface Path. (b) Bottom Surface Path.

3.3.2 Results with Same Energy Input

Since the amounts of energy input could influence phase change, unlike in 316L stainless steel, it play a critical role in S355J2G3 carbon steel. So a simulation with same energy input for all three models was created. In this simulation the energy input of the tangent model was increased and the energy input of the 90 ° model was decreased to the same as the 45 ° model.

Figure 20(a) indicates that the results are correct when the distance measured from weld toe is less than 0.8mm or larger than 1.4mm for the 90 ° model on top surface. Figure 20(b) indicates that the results are correct when the distance measured from weld toe is larger than 0.6mm for the 90 ° model on top surface. Figure 20(c) indicates that there are two zones that are invalid for the 90 ° model on bottom, one is from weld toe to 0.25mm, the other is match the rapidly increasing zone when approaching the weld toe which is between 0.4mm and 1mm. Figure 20(d) indicates that the results of the tangent model is invalid between 1mm and 1.7mm. We found that on bottom surface, the rapidly increasing zone when approaching the weld toe for any model in this study match an invalid result. On bottom surface, both the 45 ° model and the 90 ° model have an invalid result near the weld toe because of geometry change. But the tangent model did not have an invalid result near the weld toe because of no geometry change.

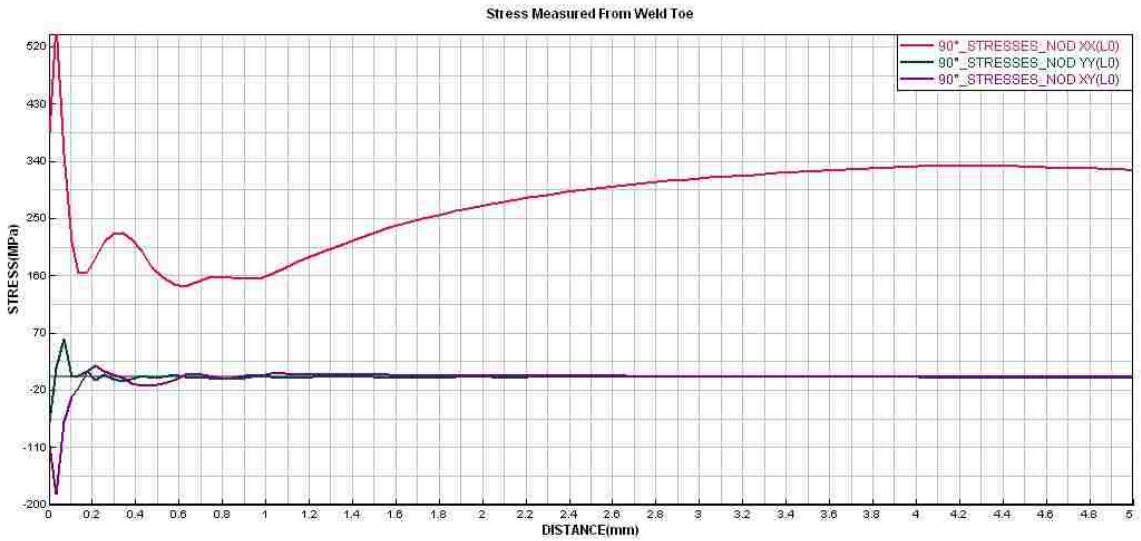
Stress Measured From Weld Toe
90°_STRESSES_NOD XX(L0)
90°_STRESSES_NOD YY(L0)
90°_STRESSES_NOD XY(L0)
STRESS(MPa)
DISTANCE(mm)

(a)

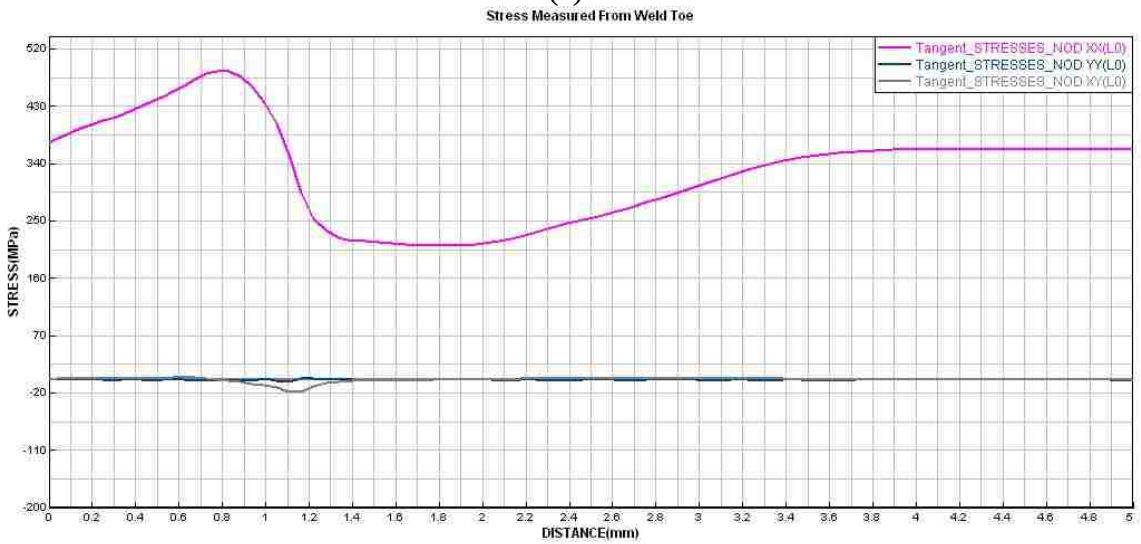
Stress Measured From Weld Toe
Tangent_STRESSES_NOD XX(L0)
Tangent_STRESSES_NOD YY(L0)
Tangent_STRESSES_NOD XY(L0)
STRESS(MPa)
DISTANCE(mm)

(b)

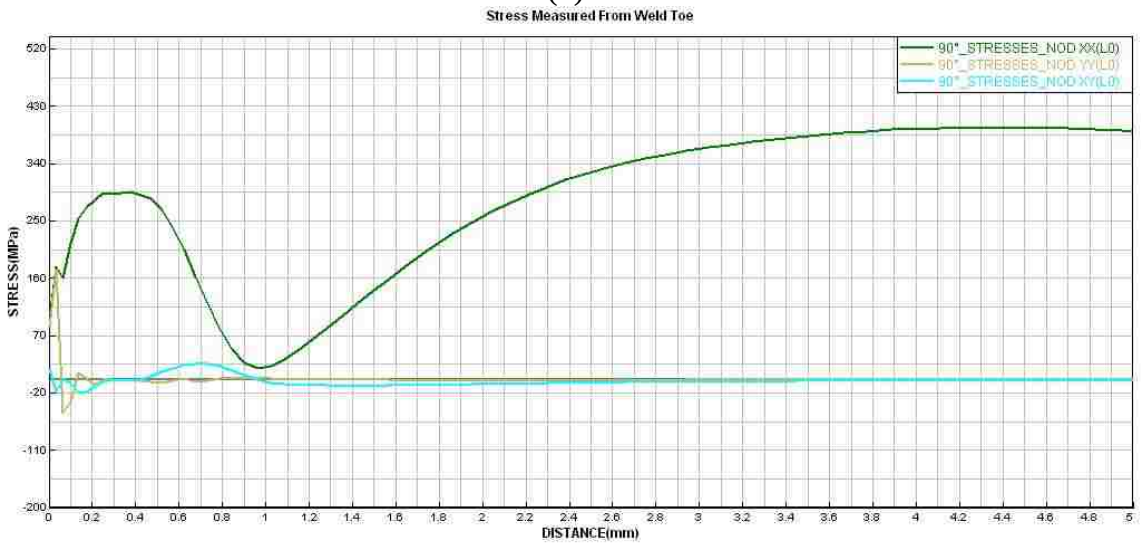
Stress Measured From Weld Toe
90°_STRESSES_NOD XX(L0)
90°_STRESSES_NOD YY(L0)
90°_STRESSES_NOD XY(L0)
STRESS(MPa)
DISTANCE(mm)

(c)

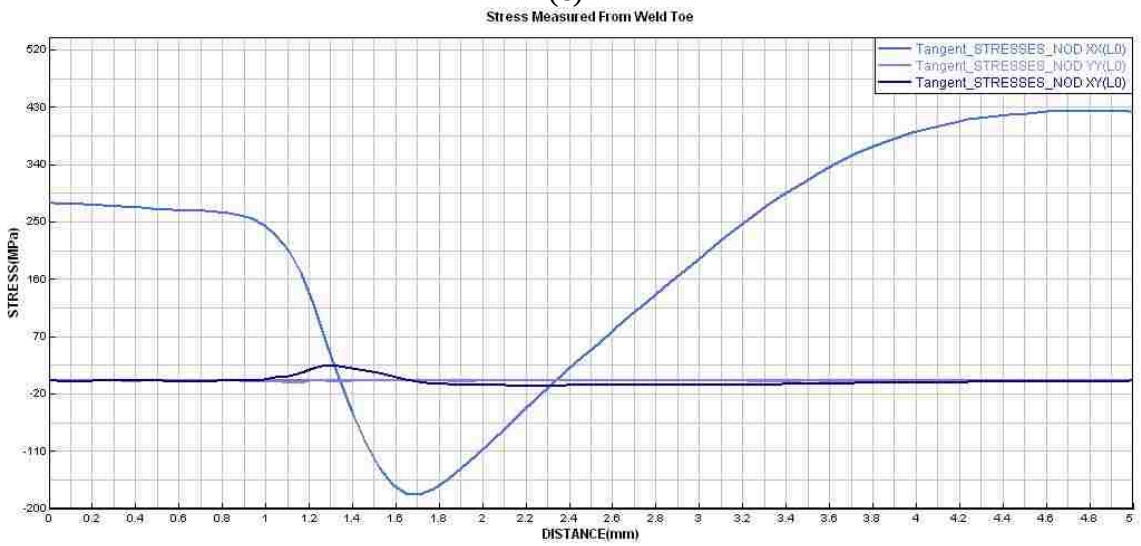

(d)

Figure 20 Stress Component of σxy, σyy, σxx Measured from Welding Toe
(a) 90 °Model Top Surface. (b) Tangent Model Top Surface.
(c) 90 °Model Bottom Surface. (d) Tangent Model Bottom Surface.

Figure 21(a) indicates the σ_{xx} stress of the tangent model is smaller than the σ_{xx} stress of the 45 ° model and the 90 ° model within 1.4mm and 3mm of the weld toe, and the σ_{xx} stress of the 45 ° model and the 90 ° model with the distance larger than 1.4mm from the weld toe are almost the same. Figure 21(b) indicates the σ_{xx} stress of the tangent model decreased first when approaching the weld toe and reaches lowest. Generally, on bottom surface, the σ_{xx} stress of the tangent model is smallest and the σ_{xx} stresses of the 90 ٩ model is largest.

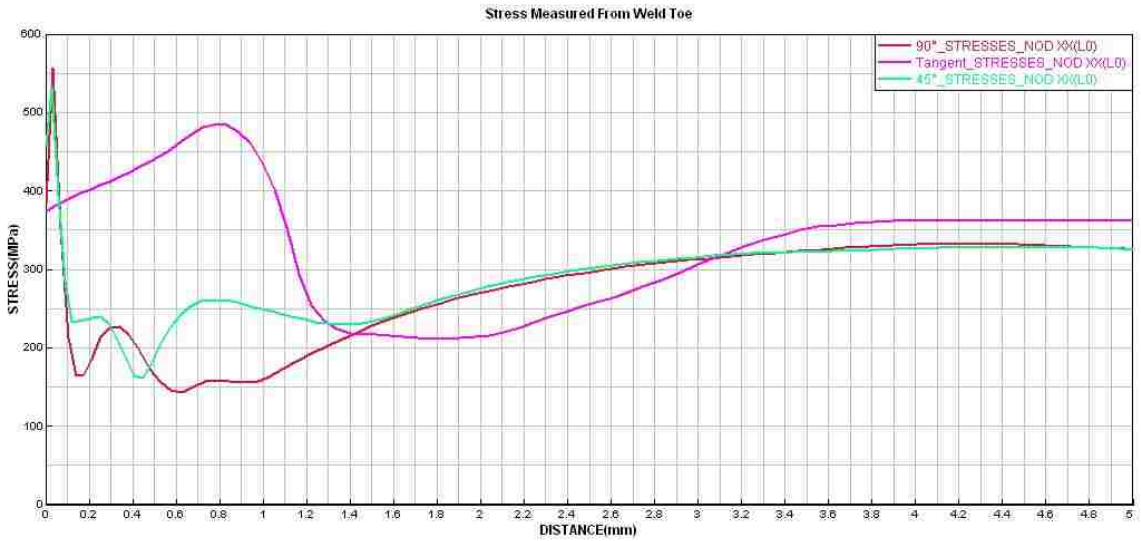

(a)

(b)

Figure 21 Residual Stress σ_{xx} Distribution Measured from Weld Toe at t=4201s with Clamp.

(a) Top Surface Path. (b) Bottom Surface Path.

Since the tangent model has smallest volume, the temperature distribution could be higher than other two models.

Figure 22 (a) shows the tangent model has most phase change along top surface path and the 90 °model has least. The 45 °model has a similar phase change distribution along top surface. It explained why the 90 °model and the 45 °model have similar stress

σ_{xx} distribution on top surface and the tangent model has smallest stress σ_{xx} within 1.4mm and 3mm of the weld toe on top surface.

Figure 22 (b) shows the tangent model has most phase change along bottom surface path and the 90 °model has least. The 45 °model has a medium phase change distribution between the tangent model and the 90 °model along bottom surface. It explained that the curves in figure (b).

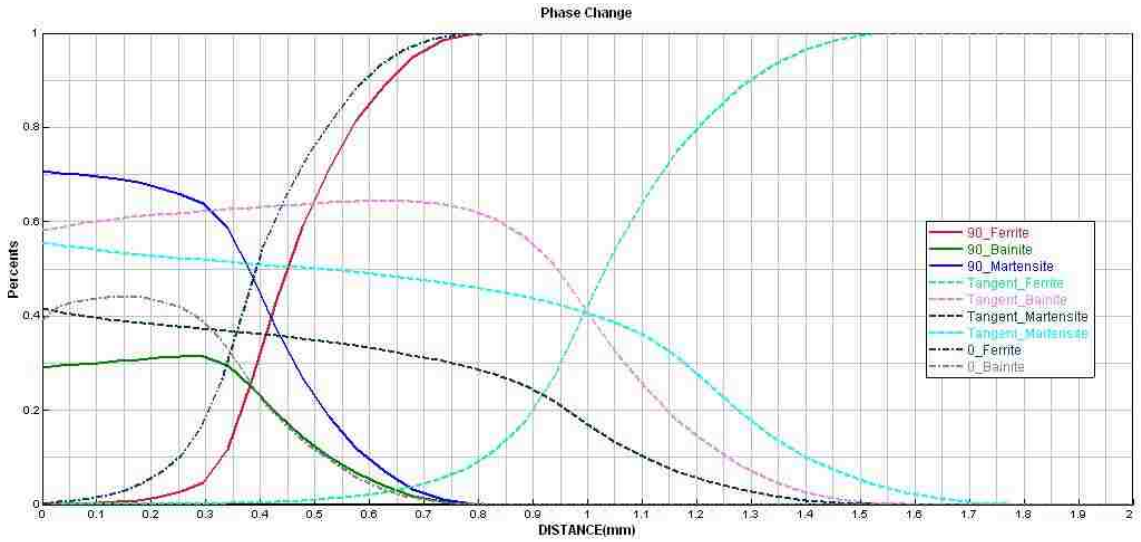

(a)

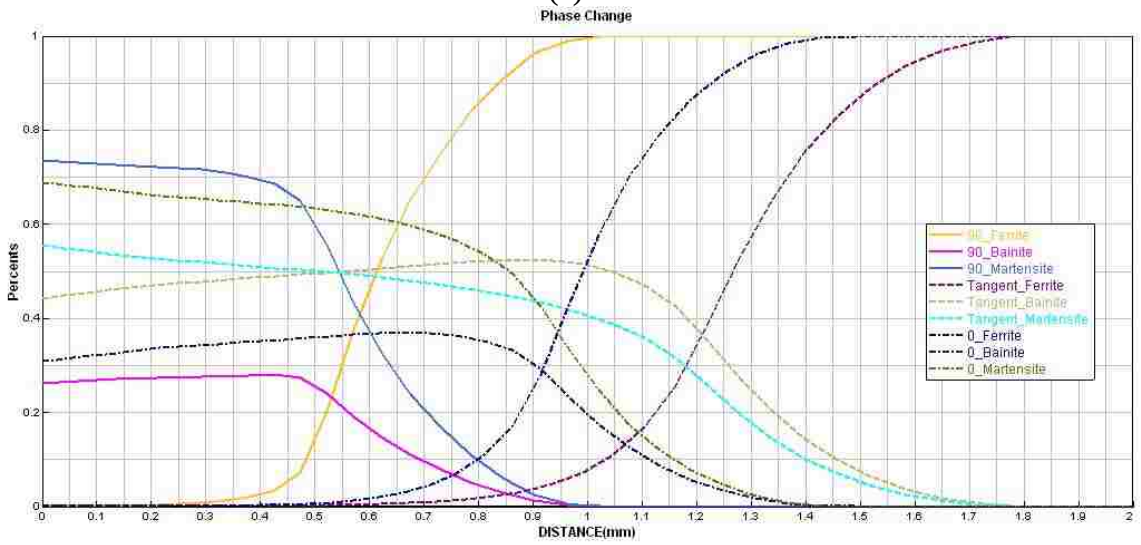

(b)

Figure 22 Metallurgical Phases Percentage of Three Models Measured from Weld Toe

(a) Metallurgical Phases Percentage of Three Models on Top Surface Measured from Weld Toe.
(b) Metallurgical Phases Percentage of Three Models on Bottom Surface Measured from Weld Toe.

3.4 Results of Tangent Models with Different Mesh Quality.

We built six tangent models with different mesh quality in 316L stainless steel. The first one is a coarse meshed tangent model which including 1583 nodes and 1664 linear elements; the second one is an average meshed tangent model which including 3766 nodes and 3978 linear elements; the third one is a refined linear meshed tangent model with 21533 nodes and 23232 linear elements; the fourth one is a refined quadratic meshed tangent model with 65621 nodes and 23892 quadratic elements; the fifth one is a coarse meshed 90 ° model with 1564 nodes and 1628 linear elements; the last one is a refined quadratic meshed 90 ° model with 40883 nodes and 13418 quadratic elements.

The computational time for first four models is approximate 2min, 4min, 20min and 29min. Results of those models are almost the same before reducing when approaching welding toe, even the mesh quality of them is so much different. Better the mesh is, closer to welding toe the curve go down. The going down points may indicate the validity of results. However, when we check the σ_{yy} and σ_{xy} stresses on the top surface. Surprisingly, σ_{yy} and σ_{xy} stresses of all models are approximately equal to zero. It means results are correct from welding toe. Possible σ_{yy} and σ_{xy} stresses cannot be used for judging those tangent model or boundary conditions will not be failure near to welding toe because of smooth contact between welding fillet and base bar. Because the going points are very close and all located within 0.3mm of welding toe. If the second explanation is true, a really simple and coarse meshed model is good enough to get good results near to the welding toe for a tangent model in 316L stainless steel. Though the

residual stress of these four models with different mesh quality is almost the same along top and bottom surface, the residual stress distribution in total model is quite different.

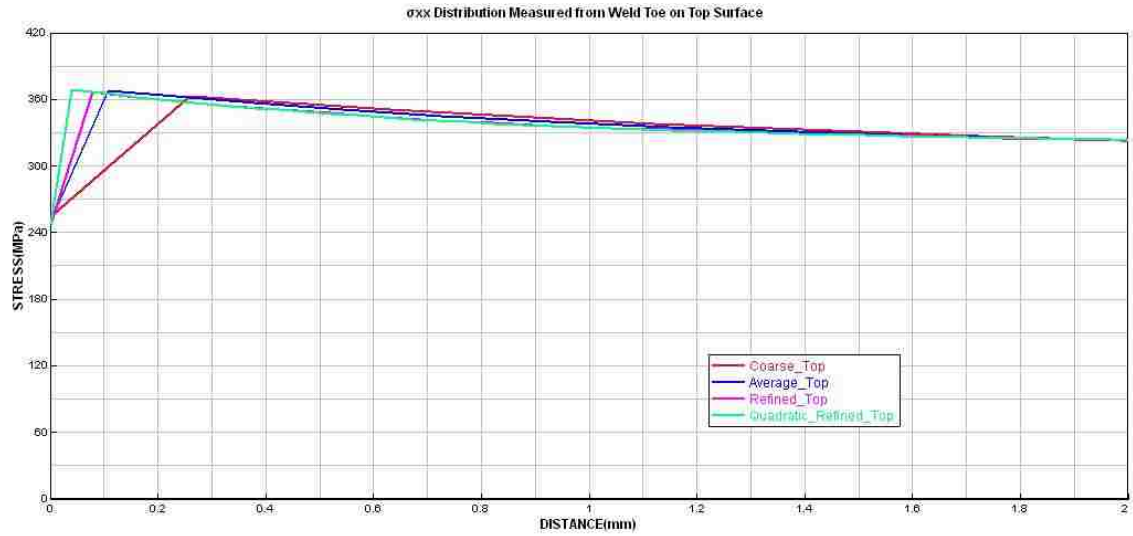

(a)

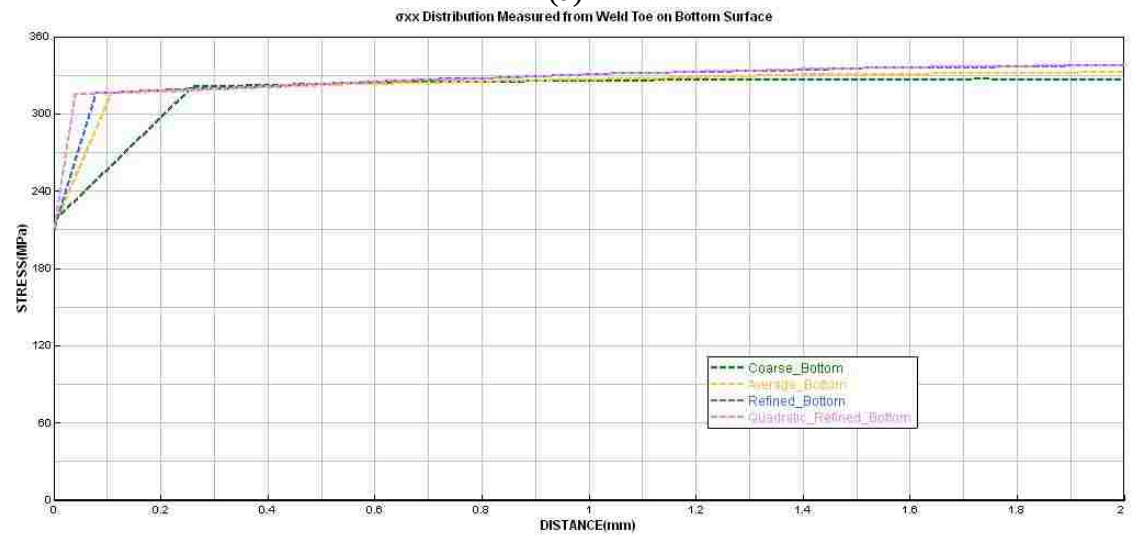

(b)

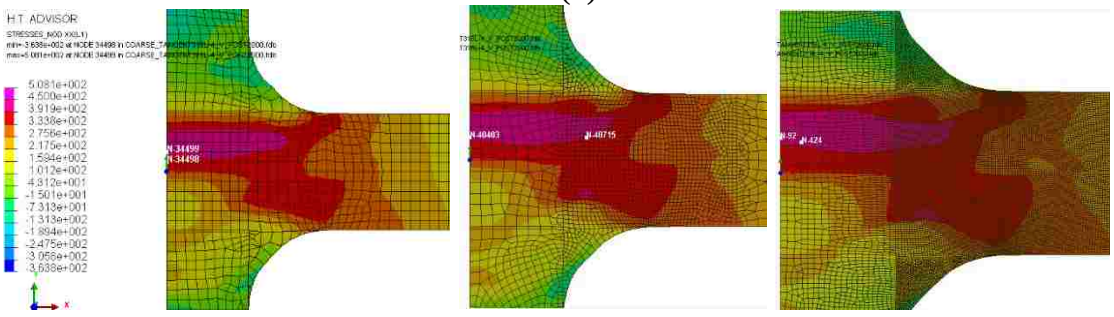

(c) (d) (e)

Figure 23 Stress σ_{xx} Distribution Measured from Weld Toe at t=4201 after Releasing Clamp. (a) Top Surface Path Measured from Weld Toe.

(b) Bottom Surface Path Measured from Weld Toe. (c) Coarse Model. (d) Average Model. (e) Refined Model with Linear Elements.

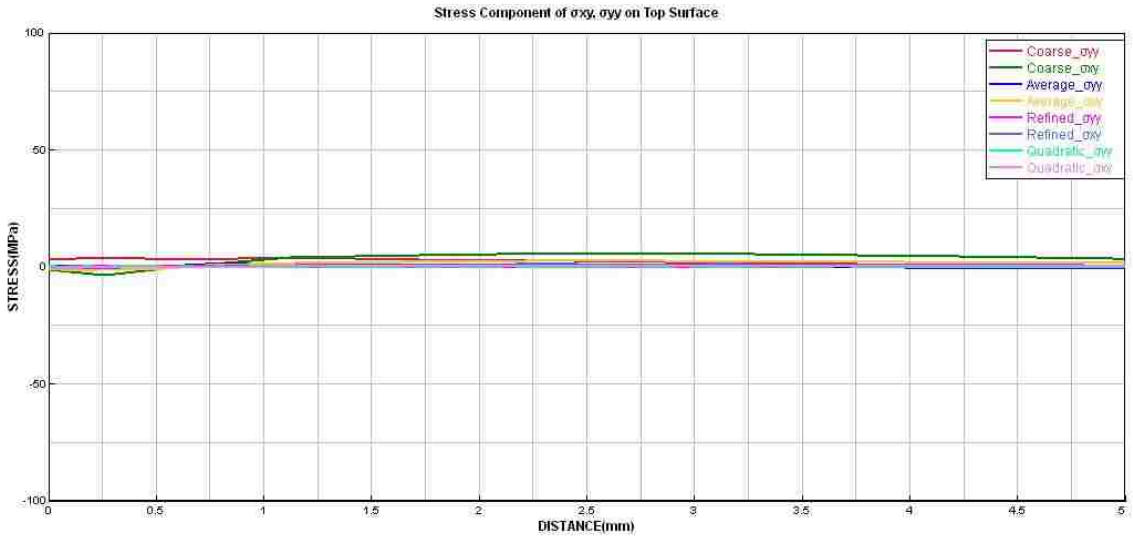

Figure 24 Stress Component of $\sigma_{xy,}$ σ_{yy} on Top Surface Measured from Welding Toe.

Results of last two models are different. The coarse model and refined model has quite different σ_{xx} curves on top and bottom surface. From figure 25(b), we know that results of coarse meshed model are incorrect within 2.75mm of welding toe and results of refined meshed model are incorrect within 0.75mm of welding toe. [6] indicates that a similar phenomenon also happens in 45° model. So we can conclude that mesh quality would influence the validity of results in welding models except for tangent model.

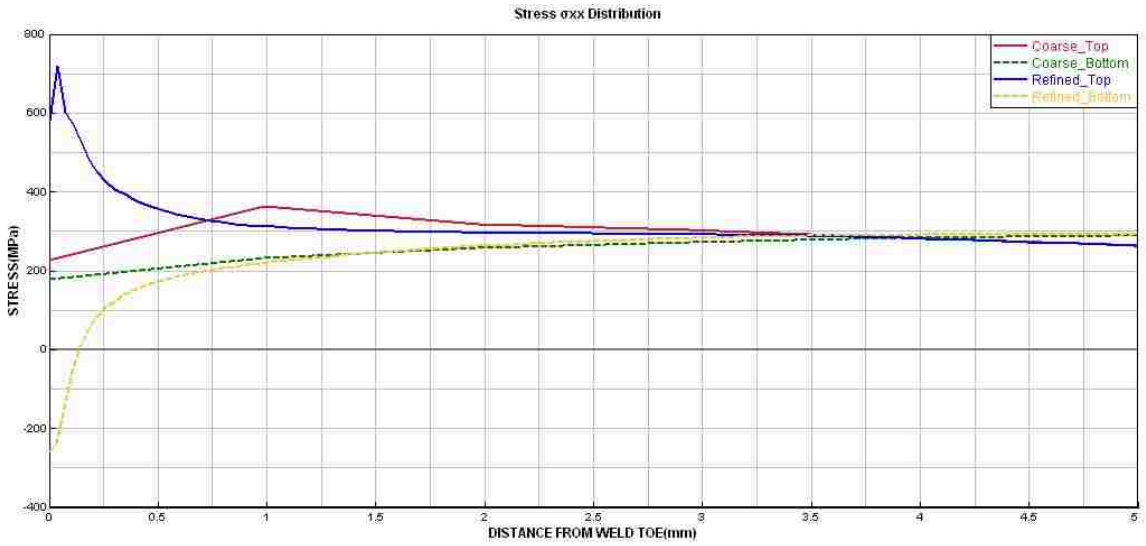

(a)

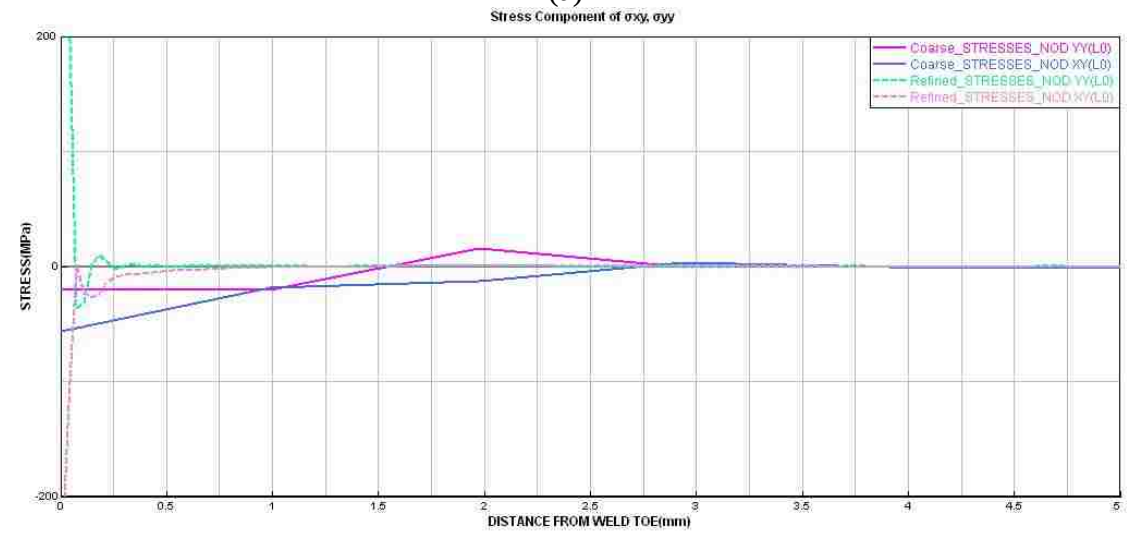

(b)

Figure 25 Stress Distribution Measured from Weld Toe at t=4201 after Releasing Clamp. (a) Stress $\sigma_{xx.}$ (b) Stress Component of $\sigma_{xy,}$ σ_{yy} on Top Surface.

Chapter 4

Conclusion

In this study, an investigation was performed to study the influence of the welding fillet geometry on the post-weld residual stresses. Of particular importance, is the stress state near the weld toe, where the geometrical stress concentration effect is most significant. This zone is also the location of important metallurgical changes, because of the phase changes that can occur in carbon steels during rapid cooling. The combined effects of stress concentration and local deviatoric stresses, due to phase changes, were the primary focus of this study. Based on results from the computational simulations, following is concluded:

1. For cases where welding is performed with different energy input (due to the different filler metal volume): fillet model with different energy input due to different fillet volume.

In the absence of clamping restraints, and no metallurgical phase changes (316L stainless steel), a tangent fillet (0 °) results in a reduced residual stress near the weld toe when compared with fillet models that have a larger contact angle, e.g., 45 ° and 90 °. This is an expected result due to the stress concentration that increases with increasing contact angle.

In the numerical simulations with remote clamp conditions and no metallurgical phase change, the residual stresses near the second weld decrease and the stresses near the first weld increase in magnitude, after releasing the clamping restraints. The larger the

contact angel between the fillet and the base bar, the larger the change in the residual stress.. This again was expected, since the release of the clamp restraint introduces an elastic springback that superimposes a bending stress through the flat plate's cross-section.

It can be concluded that the tangent fillet model is less sensitive with clamp condition.

For the results obtained from carbon steel (S355J2G3), where metallurgical phase changes are important, and the clamp condition is enforced, a smaller contact angel shows a reduction in the residual stresses after releasing clamp.

It appears that the metallurgical phase change, combined with a larger plate contact angle, results in a larger HAZ, reducing the residual stress near the weld toe.

It was shown that mesh refinement does not improve the accuracy of the results for the tangent fillet model, i.e., the results seem to have converged with the least refined finite element mesh However, it was shown that increased meshed refinement is required for larger fillet weld contact angles, due to the more severe stress concentration that is introduced, to obtain higher accuracy results.

2. For cases where welding is performed with same energy input: Different fillet model has same energy input.

316L stainless steel models are insensitive to energy input.

Smaller volume of fillet cause a higher peak temperature and bigger phase change zone on top and bottom surface which could reduce residual stress.

Reference

[1] Messler, R. W., Jr., Principles of Welding, Wiley-Interscience, 1999.

[2] Berge, S., and Eide, O. I., Residual Stress and Stress Interaction in Fatigue Testing of Welded Joints, in Residual Stress Effects in Fatigue, ASTM Technical Publication 776, ASTM 1916 Race Street, Philadelphia, PA, 19103, 1981, pp. 115-131.

[3] Baumgartner, J., and Bruder, T., Influence of Weld Geometry and Residual Stresses on the Fatigue Strength of Longitudinal Stiffeners, Weld World, Published Online: 12 July, 2013.

[4] William, M. L., Stress Singularities Resulting from Various Boundary Conditions in Angular Corners of Plates in Extension, Trans. ASME, J. of Applied Mech, Vol. 19, 1952, pp. 526-528.

[5] Bussu, G., Irving, P. E., The Role of Residual Stress and Heat Affected Zone Properties on Fatigue Crack Propagation in Friction Stir Welded 2024-T351 Aluminium Joints, International Journal of Fatigue, 2003

[6] Nied, H. F., and Siegele, D. Study of the Influence of Material and Welding Modeling on the Residual Stresses in Longitudinal Stiffeners, Commission XIII Fatigue of Welded Components and Structures XIII-2479-13, 2013.

[7] Goldak, J. A., and Akhlaghi, M., Computational Welding Mechanics, Springer, 2005.

[8] Rybicki, E. F., and Stonesifer, R. B., Computation of Residual Stresses due to Multipass Welds in Piping Systems, ASME J. Pressure Vessel Technology, Vol. 101, 1979, pp. 149-154.

[9] Lindgren, L. E., and Karlsson, L., Deformatkion and Sttresses in Welding of Shell Structures, Int. J. Numerical Methods in Engineering, Vol. 25, 1988, pp. 635-655.

[10] Yildirim, B., and Nied, H. F., Residual Stresses abnd Distortion in Boiler Tube Panels with Welded Overlay Cladding, ASME J. Pressure Vessel Technology, Vol. 126, 2004, pp. 426-431.

[11] Price, J. W. H., Ziara-Paradowska, A., Joshi, S., Finlayson, T., Semetay, C., and Nied, H. F., Comparison of Experimental and Theoretical Residual Stresses in Welds: The Issue of Gauge Volume, Int. J. of Mechanical Sciences, Vol. 50, 2008, pp. 513-521.

[12] SYSWELD 2010, Reference Manual, www.esi-group.com, Release January 2010.

[13] Nied, H. F., Welding Simulation Using SYSWELD: An Introductory Tutorial, 2013.

[14] HyperWorks Desktop User's Guide, 2012

[15] Budynas, R. G., Advanced Strength and Applied Stress Analysis, 2001

Vita

Chao Zhang was born on April 18, 1990 in Wenzhou City, Zhejiang Province to his parents, Wenhua Zhang and Xingmeng Lin. He resided in Hanzhou City, Zhejiang Province and attended The High School Attached to Zhejiang University. In August 2007, he was accepted to Zhejiang University and graduated with a BS degree in July 2011. He was awarded high honor student for all eight semesters of his undergraduate study. After Graduating from Zhejiang University, he took park in an internship in Hangzhou Great Star Industrial CO., LTD. In September, 2012 he started his graduate study in Mechanical Engineering and Mechanics Department, Lehigh University.